RHEINISCHE FACHHOCHSCHULE KÖLN
University of Applied Sciences

Department: Engineering Sciences
Course of studies: Technical Management (M.Eng.)

Master Thesis

Development of a Measurement Method for Continuous Quantification of Heat Transfer Fluid Vapor in Air

presented by: Marcel Hardelt
mat.-no. 131202018

1. Examiner: Prof. Dr. Sebastian Mader
2. Examiner: Prof. Dr. Ulrich Russek

Supervisor: Dr. Alejandro García Segura
Dr. Eckhard Lüpfert
(DLR - Institut für Solarforschung Köln/Almería)

winter semester 2022/23

Abstract

Parabolic trough solar power plants use heat transfer fluids up to around 400°C flowing for energy collection through the absorber tube. While the fluid is toxic, environmentally harmful and flammable, the flexible pipe connectors at the ends of each parabolic trough solar collector are a critical risk for leakage because they are exposed to intermittent thermal and mechanical loads. To reduce the environmental impact by bleeding through sliding seals of the connectors, it is a goal of ongoing technical developments to quantify the leakage rate of these connectors with a suitable measurement system in order to compare different connector technologies, sealing types, development stages, and deterioration over time (condition monitoring).

In this work a measuring method for the determination of the commonly used organic heat transfer fluid concentration in air was developed, to be used in a measuring system for leakage quantification. For this purpose, an experimental setup was created with which the properties of the vapor to be detected could be investigated under different ambient conditions. Subsequently, two sensors were qualified with regard to the quantification of the concentration, and the sensor properties were investigated using the setup. A prototype of the measurement system was used to ensure the suitability of the sensors for the specific measurement application.

Table of contents

1 Introduction

The effects of the human-induced climate change can already be observed in the form of coral bleaching, the rise of the sea level and increases in the number and intensity of extreme weather events (Pörtner et al., 2022, p. 8). At the same time, economic and population growth leads to a rising electricity demand (Cozzi et al., 2020, p. 55), most of which is still obtained from fossil fuels (Schiffer et al., 2021, p. 34 f.). According to the executive director of the *International Energy Agency* (IEA), Dr. Birol “only faster structural changes to the way we produce and consume energy can break the emissions trend for good” (Fatih, 2020). Concentrating solar power (CSP) is a pioneering technology to generate climate-neutral energy from an inexhaustible, sustainable energy source. The world map shown in Figure 1.1 provides an overview of the distribution of average solar radiation, considering that Direct Normal Irradiation (DNI) is a key parameter that directly influences the efficiency of CSP plants and therefore the place where they are more favourable to be located.

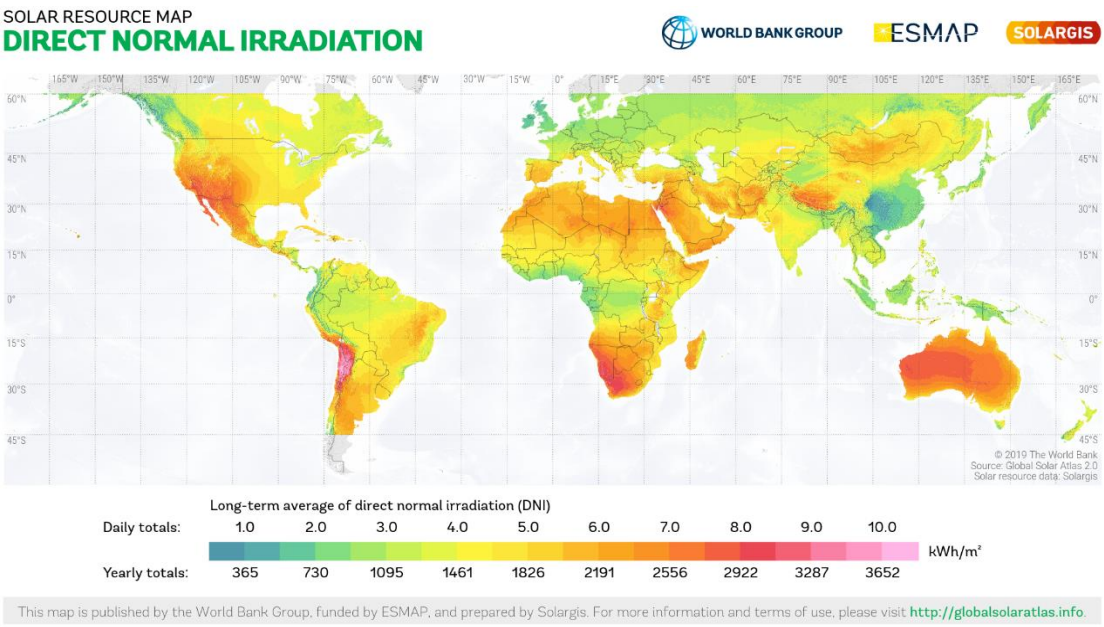

Figure 1.1, Solar Resource Map - Direct Normal Irradiation
Source: (The World Bank, 2019)

CSP systems use solar radiation by focusing the direct sunlight reflected from mirrors onto a receiver, where the concentrated radiation is absorbed and transferred to thermal energy [IRENA, 2021, p. 106]. To track the path of the sun during the day, the mirrors are regularly realigned by a drive system. With the help of a heat transfer fluid (HTF), the heat is transported to the power block, where it is converted into electrical energy. Depending on the used HTF, it can either directly drive a heat engine or transfer the heat to a steam generator that powers a steam engine. (Heller, 2017, p. 1,5)

With regard to the energy transition towards renewable energies, CSP can play a significant role. Whereas photovoltaic (PV) and wind power systems can only produce electricity under suitable weather conditions, CSP plants are commonly equipped with a large thermal energy storage (more than 1 GWh capacity). As a result, electricity can be generated on demand and thus compensate for fluctuations in the grid. However, utility-scale battery storages are less cost efficient and have limitations in terms of storage duration. (IRENA, 2021, p. 116)

Although the levelized cost of electricity[1] (LCOE) of CSP plants with thermal storage is currently still about twice as high as that of modern wind power plants or photovoltaic systems, a significant reduction in costs is expected through further development and mass production. In fact, the LCOE of solar thermal power plants has fallen by 68% between 2010 and 2020. (DLR, 2021, p. 16 ff.; IRENA, 2021, p. 113)

The different technologies of CSP plants can be classified into two classes, namely line- and point-focusing systems. Central receivers (also called solar power towers) and parabolic dish collectors focus the solar radiation on a single point. This way, the systems can achieve concentration factors of over 1000. In contrast, parabolic trough collectors (PTC) and linear Fresnel reflectors concentrate the sunlight to a receiver tube, which is mounted in the focal line of the mirrors. These systems can reach concentration factors of up to 100. Line-focusing systems only need a single-axis tracking (Pitz-Paal, 2020, p. 413 f.). Figure 1.2 depicts a schematic representation of the four main CSP technologies.

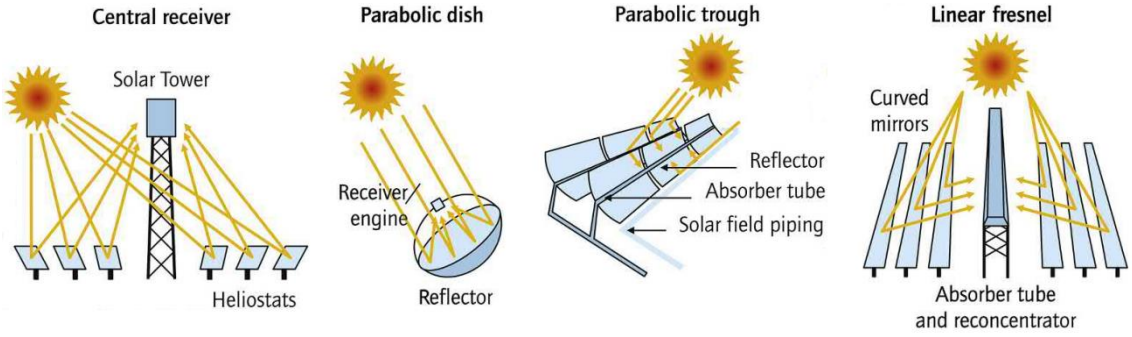

Figure 1.2, Technologies for concentrating solar radiation
Source: (Pitz-Paal, 2020, p. 414)

Parabolic trough is the solar thermal technology with the highest cumulated capacity in worldwide commercial installation (around 5 GW), it is considered the most affordable

---

[1] Levelized cost of electricity is a tool for comparing the cost efficiency of different electricity generation technologies by dividing the total cost by the generated electricity over their lifetime (Arinaldo & Pujantoro, 2019, p. 5).

and least risky technology (Lovegrove & Stein, 2021, p. 239). Since the first commercially used CSP plants started operation in 1986, the PTC technology has been continuously developed and optimized, resulting in a wide variety of component designs (Mehos et al., 2020, p. iii). As a result, the Qualification and Systems Department of the Institute of Solar Research of the DLR (German Aerospace Center) is working on the development of uniform test conditions for testing the key elements of PTC systems. One of the components regarded as a key element is the flexible pipe connector, the so-called rotation and expansion performing assembly (REPA), which is the linking element between the moving absorber tube in the collector and the fixed ground piping. Since currently used REPAs have at least one dynamic seal in which the sealing surfaces experience a cycling movement relatively to each other, they are particularly prone to smaller leaks (bleeding) or failures with escaping HTF. Because of the environmental harmfulness and toxicity of the HTF, the tightness of these components is an important factor that must be considered in the study of REPA leakages under realistic conditions.

A measurement concept for the quantification of small leakages was already developed in the run-up to this master's thesis, considering the particular boundary conditions at the measurement location. The concept consists in generating an air flow that passes around the REPA before entering the measuring section. At the same time, the hot HTF that may exit the system would evaporate due to the pressure drop and be carried by the airstream into the measuring section. This is where the mass flow and the concentration in the airstream would be measured, from which the leakage flow can be ultimately determined. (Hardelt, 2022, p. 23)

The present work aims at selecting and qualifying a suitable measurement method for continuous quantification of gaseous HTF in air, which can be used in a leak measurement system.

2 State of the art

This chapter summarizes the technology of parabolic trough solar power plants and provides the fundamentals for the current research project. The basic design and mode of operation of the systems are described, and the tasks and properties of the REPAs and the heat transfer fluids are explained. Subsequently, leakages at REPAs are discussed and the steps already taken for the development of a leakage measurement system listed. Accumulated knowledge gained from the development process is presented, forming the basis of the present work. This includes the design of the leakage measurement system as well as the experience with HTF sensors. Finally, the physical properties of the HTF to be measured and the basics of concentration measurement are explained.

2.1 Parabolic trough solar power plant

A solar thermal power plant with PTC technology can be divided into three sub systems. The solar field, consisting of many collectors (e.g. 624 collectors in a Spanish 50 MW plant), gathers the energy of the solar radiation and converts it into thermal energy. The power block transforms the thermal energy into electrical energy, which is be fed into the power grid. The third element is the thermal storage unit, acting as a buffer between the solar field and the power block, loading thermal energy, as needed, or unloading it to the power block. These three subsystems are connected by pipes, through which the HTF is pumped. Figure 2.1 illustrates the schematic structure of a parabolic trough solar power plant.

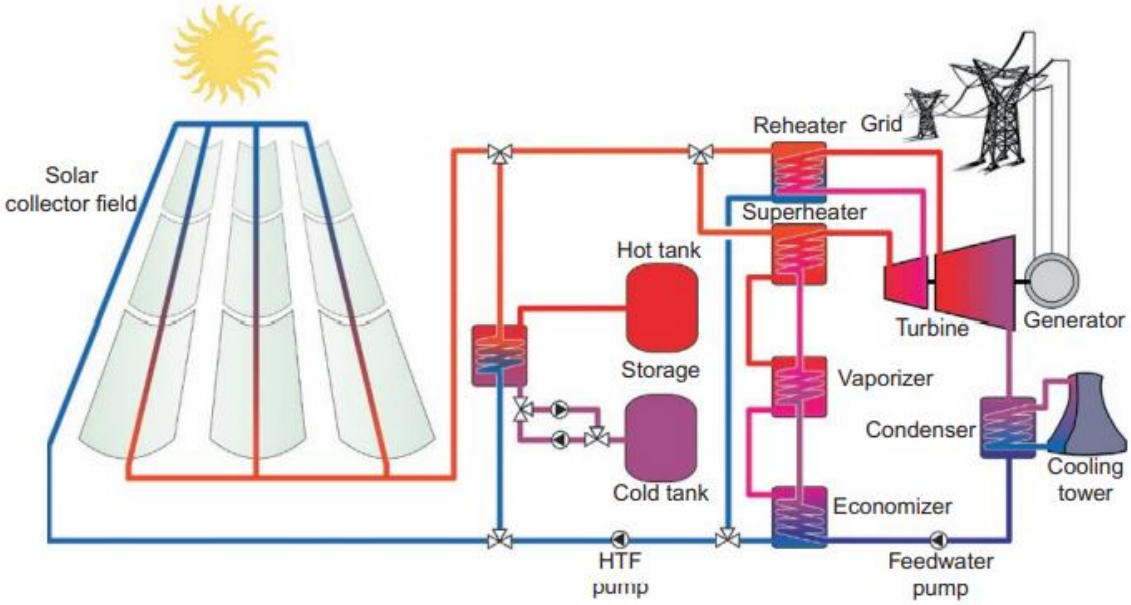

Figure 2.1, Schematic of a parabolic trough power plant
Source: (Heller, 2017, p. 5)

The PTCs of a solar field are arranged in parallel rows. Collector modules (here 12 m by 5.8 m) are connected to each other and form the collector as shown in Figure 2.2. In the center of each PTC there is a hydraulic drive system that precisely tracks the collector around its longitudinal axis in order to focus the sun. Due to better efficiency, collectors are usually installed in north-south orientation and thus track the solar azimuth angle with the axial rotation (Sun et al., 2020, p. 5). The HTF flowing through the pipe in the focal line transports the generated heat to the power block or to the storage tank.

Figure 2.2, Solar collector at Plataforma Solar de Almería (owned by CIEMAT)

In the power block, thermal energy is converted into mechanical work using the thermodynamic Rankine cycle. For this purpose, the hot HTF pre-heats water in several stages, evaporates it and then superheats the steam at a typical pressure of 100 bar. This steam drives a turbine and is then cooled down in a condenser reaching a pressure below 0.1 bar. The feedwater pump pressurizes the water back into the heating section. A connected generator converts the mechanical work of the turbine into electrical energy, which is fed over a transformer into the power grid. (Pitz-Paal, 2020, p. 417)

The main task of storage is to compensate for fluctuations in solar radiation and in the demand for electrical energy, in particular for evening and night time. Thus, the storage system contributes to the stability of the electricity grid and protects the turbine from damage due to unstable steam parameters. Even if the storage is not essential for the operation of the plant, the advantages clearly outweigh the costs, so that modern PTC plants are equipped with storage. (Lovegrove & Stein, 2021, p. 236 ff.)

Thermal energy storage usually consists of two tanks for molten salt ($NaNO_3$ and KNO_3 mixture) and a heat exchanger. During periods of high energy output from the solar field, part of the HTF flows through the heat exchanger, transferring thermal energy to the salt, which is pumped from the cold tank to the hot tank. If electric energy demand from the grid is higher than provided by the solar field, the salt flow and HTF flow in the heat exchanger are reversed and the thermal energy is used to generate electricity in the power block. (Pitz-Paal, 2020, p. 417)

2.1.1 Parabolic trough collector (PTC)

The collector has the task of transferring the energy of the sun's rays into the HTF. For this purpose, the curved mirrors are arranged in the shape of a trough, which has the form of a parabola in its cross-section. As a result, the sunlight incident on the mirrors parallel to the plane of symmetry of the trough is focused on a focal line. In this line is the receiver, consisting of a steel pipe of typically 70 mm diameter and a concentrically arranged glass tube. Between these tubes there is vacuum to reduce heat loss by convection. The incoming solar rays are absorbed on the steel pipes surface and the heat energy is then transferred to the HTF, flowing through the pipe. (DLR, 2021, p. 13)

Modern collectors have parabola widths of 5.78 up to 8.2 m and lengths of 100, 150, or up to more than 200 m, so they consist of a large number of curved mirrors. The precise alignment of the mirrors is crucial for the efficiency of the collector, while the mirrors are exposed to strong loads in windy conditions. They are held in place by a rigid metal framework structure. The receiver tube mounting allows thermal expansion in axial direction. (Lovegrove & Stein, 2021, p. 226 ff.)

2.1.2 Rotation and Expansion Performing Assembly (REPA)

The flexible pipe connector, often called REPA, is the interconnecting element between the ground piping, which distributes the HTF over the solar field, and the receiver tube, located in the focal line of the PTCs. As the PTC follows the motion of the sun throughout the day, the receiver tube goes around the axis of rotation of the SCA. In addition, the thermal expansion of the receiver tube causes an axial movement of its connection point. These movements are enabled by the REPAs located on both ends of a collector. (León et al., 2018, p. 1 f.)

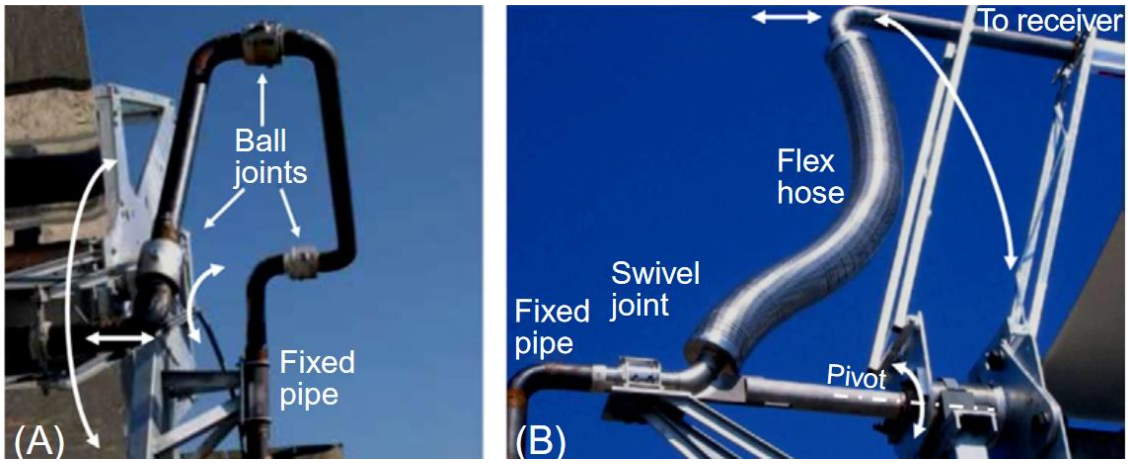

Figure 2.3, Rotation and expansion performing assemblies: ball joint assembly (left), rotary flex hose assembly (right)
Source: (Heller, 2017, p. 218)

REPAs are designed to introduce the lowest forces possible while providing a leak-tight connection between the ground piping and the receiver tube. There are various approaches to achieving this, either using combinations of ball joints or swivel joints and flex hoses. The first power plants used only corrugated hoses without swivels as REPA, but they often failed due to their sensitivity to torsional forces. Therefore, so-called ball joint assemblies were applied further on, see left side of Figure 2.3 (Mehos et al., 2020, p. 145). They are state of the art and the most widely used REPAs in large scale CSP, along with so-called rotary flex hose assemblies, which combine a corrugated hose with a swivel joint, as shown on the right side of Figure 2.3 (Plumpe, 2016, p. 17).

The swivel joint of the rotary flex hose assembly is mounted in line with the rotational axis of the SCA and has the task of enabling the rotational movement. It eliminates the torsional stresses and thus protects the corrugated hose. In addition, a torque sword, connected to the pipe bend between the swivel joint and the flex hose, transmits the necessary torque to turn the swivel joint. This further reduces the forces acting on the flexible hose and also the radial forces on the swivel joint coming from the expansion of the flex hose.

The ball joint assembly is a combination of three ball joints connected by pipes. In contrast to the swivel joints, which only enable rotatory movements, the ball joints can additionally perform tilting movements of few degrees (17 °) (ATS, 2021, p. 2). This combination allows them to compensate for both the rotary motion and the thermal expansion of the receiver tube. The advantage of the ball joint assemblyr is a lower pressure drop. The compressed graphite powder seal used in the ball joints requires regular maintenance and is more prone to leakage. (Sniderman, 2011)

Due to the complex movement in combination with the high operating temperature, these connecting elements are one of the critical components of a PTC power plant. To contribute the study of REPAs, the DLR in cooperation with the *Centro de Investigaciones Energéticas, Medioambientales y Tecnológicas* (CIEMAT) built a test rig for performing durability tests on these components. The REPA test rig, installed at the *Plataforma Solar de Almería* (PSA) in Spain, is designed for accelerated aging of REPAs under realistic conditions and is able to simulate their lifetime of 10'000 cycles over 30 years within a few weeks (Heller, 2017, p. 218 f.).

2.2 Heat transfer fluid (HTF)

The HTF has a major impact on the efficiency and profitability of the power plant. The suitability of a substance to be used as an HTF depends on many properties. These include high thermal stability for use at high temperatures, with the objective of high steam turbine efficiency. High thermal conductivity is advantageous for heat transfer in the receiver tubes and in the heat exchangers. In addition, high specific heat capacity and low viscosity reduce energy consumption of the pump. The environmental compatibility and toxicity of the HTF, as well as the aging and disposal possibilities are also of great importance. With regard to the initial costs of the power plant, attention must be paid to both the price of the HTF itself and to the installation requirements for the piping components depending on vapor pressure and corrosion aspects. (Krishna et al., 2020, p. 29; Solartechadvisor, 2022)

The commercially deployed PTC plants have typically used as HTF a synthetic oil consisting of a eutectic mixture of two organic hydrocarbon sybstances: 73.5% diphenyl oxide ($C_{12}H_{10}O$) and 26.5% biphenyl ($C_{12}H_{10}$) (BP/DPO). The main characteristics of this synthetic oil are explained hereafter. First, its application temperature range is between 12 °C and 400 °C (Dow Chemical Company, 2022; Eastman, 2019). Since the boiling temperature of the fluid at ambient temperature is 257 °C, the HTF circuit must be operated under pressure of 20-30 bar (Lovegrove & Stein, 2021, p. 251 f. Grirate et al., 2016, p. 2). Its high thermal stability decreases beyond approx. 400 °C, resulting in its decomposition into gaseous substances, including hydrogen, carbon monoxide and benzene (Grirate et al., 2016, p. 2; WACKER, n.d.; Lang & Lee, 2015, p. 679). To avoid its crystallization (below 12 °C) ambient temperature, a freeze protection in form of continuous circulation and heating is required. The environmental and health hazards posed by its components and decomposition products represents another disadvantage (Eastman, 2020). These substances are toxic by skin contact or inhalation and can self-ignite in presence of oxygen (Eastman, 2020; Mir-Artigues et al., 2019, p. 76). Still, it remains the

most commonly used HTF due to its good thermo-physical properties, conductivity and specific heat capacity, as well as the extensive experience and good scalability of the power plants in which it is used.

Numerous other liquids, gases and two-material systems have also been considered and investigated for their suitability as HTFs. Silicone oils, for example, allow the receiver output temperature to be increased to 425 °C (Lovegrove & Stein, 2021, p. 251 f. Jung et al., 2015, p. 665). At the same time, they have a lower freezing point of below -40 °C, which eliminates the need for an antifreeze device (Hilgert et al., 2019, p. 1). Furthermore, it exhibits significantly better environmental compatibility and lower health hazards (Hilgert et al., 2019, p. 1). Due to the similar operating temperatures and similar flow properties, silicone oil can replace BP/DPO without major changes to the power plants. However, only few plants are equipped with this HTF because of the higher price and steam pressure combined with the novelty of this development (Lovegrove & Stein, 2021, p. 251 f.).

Molten salts are already being used in solar tower power plants or in the thermal storage systems of parabolic trough power plants. In this case, their high operating temperature of up to 570 °C and low vapor pressure are key advantages. They are also less expensive than conventional thermal oils and have a lower environmental impact. Their main disadvantage with regard to the use as HTF in parabolic trough power plants is the high freezing point of up to 230 °C, requiring a more powerful freeze protection than for thermal oil. In addition, the corrosiveness of the salts is problematic. (Benoit et al., 2016, p. 306 ff. Krishna et al., 2020, p. 9 ff.)

The use of water as HTF with direct steam generation (DSG) inside the HCE is very attractive due to the saving of heat exchangers in the power block and the resulting reduction of thermal losses (Lovegrove & Stein, 2021, p. 251; Montes et al., 2010, p. 4; Krishna et al., 2020, p. 9). With DSG, temperatures greater than 500 °C can be achieved, hence a more efficient operation of the steam turbine (Zarza Moya, 2017, p. 79). In addition, the environmental compatibility of water and its low price are further advantages (Krishna et al., 2020, p. 8; Zarza Moya, 2017, p. 79). However, due to the phase change DSG is not compatible with conventional thermal molten salt storage, thereby losing a major advantage of CSP technology (Zarza Moya, 2017, p. 79 f.). Moreover, at steam temperatures of 500 °C, working pressures of about 100 bar are required and lead to increased costs for more stable pipes, HCEs, and connectors (Lovegrove & Stein, 2021, p. 251; Montes et al., 2010, p. 6). The two-phase condition of the water poses another problem. Due to the large decrease in density during the evaporation process, the flow

velocity and thus the pipe friction increases by a multiple. This complicates the regulation of the parallel connected collector rows and requires higher control effort (Zarza Moya, 2017, p. 79; Krishna et al., 2020, p. 9).

2.3 Leakage of REPAs

A leak is a structure in the wall of an object that is capable of allowing a medium to pass from one side of the wall to the other. These structures can be holes, cracks or porosities as well as, for example, defects or gaps in the atomic lattice. Since there are no defect-free bodies, there are no absolutely tight objects and thus tightness depends on the requirements of the system. The leakage rate, which describes the throughput of a medium through a leak, can be expressed as mass, molar or volume flow rate, although in the latter case a reference pressure must also be specified for compressible media. This rate is mainly dependent on the pressure or concentration difference between both sides of the wall, the geometry of the leak and the flow properties of the medium. (Pfeiffer Vakuum, 2014, p. 6 ff.)

In parabolic trough power plants, most of the junctions of pipework are welded and exhibit a technically tight connection when the welds are intact. There are also high quality standards regarding flanged joints with gaskets, such as those used for inserted sensors, valves, or pumps, especially in chemical plants (Bathen et al., 2000; Omiya & Sawa, 2014). However, in a best practice study by the National Renewable Energy Laboratory (NREL) which compiled the experiences of CSP plant owners, operators, mechanics and stakeholders, leakage from REPAs was reported to be a major problem (Mehos et al., 2020, p. 20). Considering frequency of occurrence and impactlevel, it was the second largest issue of concern, and one power plant operator reported losing up to 2% HTF annually, mainly due to ball joint leakage (Mehos et al., 2020, p. 20, 145).

This problem can be understood by examining the sealing systems in the REPAs. In the case of ball joints, it is a hollow ball sitting in a housing and held in place by two metal sealing rings. In the cavity between the rings there is graphite powder, compressed by a screw and serving as a seal (ATS, 2021, p. 2). The swivel joint of the rotary flex hose assembly consists of a tube shaft inserted into a housing. A bead on the shaft sits in a joint inside the housing and is guided by two sealing rings. One of these sealing rings is static and the second one is pressed against the bead by a spring. Due to this relative movement between the sealing surfaces of the ball and swivel joints, they are more prone to leakage than flanged connections (Persson & Yang, 2008, p. 10). In addition, it is not possible to apply the same surface pressures between the sealing surfaces of the

REPAs as with flange seals, because this would result in large frictional forces when the REPAs are moved.

The best practice study showed that swivel joints usually do not leak noticeably, whereas ball joints show significant leakage more frequently. However, this can be reduced drastically with regular maintenance by pressing new graphite into the ball joints at 4 – 5 year intervals. In contrast, the swivel joints do not require any maintenance. (Mehos et al., 2020, p. 4, 106, 145)

The thermal fluid is kept liquid inside the piping by applying a working pressure higher than the vapor pressure, despite exceeding the boiling temperature. However, when escaping from a leak, the HTF evaporates due to the pressure drop (Solutia, 1999, p. 6). It dissipates in the surrounding air. However, when the concentration of HTF in the air exceeds the saturation concentration, HTF droplets deposit in the air and form a visible wet vapor.

HTF leakage represents a financial loss and a danger to operators as well as the environment. An average solar field with 120 collector loops has 960 REPAs in use (Hilgert et al., 2015). This is why the leak-tightness of swivel and ball joints should be further investigated and improved.

2.4 Leakage quantification systems

Portable chemical sensors are used on the solar fields to detect gaseous BP/DPO. With these sensors, leaks can be detected before vapor becomes visible (Lovegrove & Stein, 2021, p. 257). The detection limit is highly dependent on the distance to the leak and the wind conditions. Furthermore, no quantitative statement can be made about the leakage rate.

As part of the REPA Guideline project (BMWK founded, 7. Energieforschungsprogramm) generally dealing with the technical development on REPAs and the definition of a standardized test procedure, the leakage measurement project is dedicated to the development of a measurement system for quantifying the leakage rate of REPAs under working conditions. A concept for this measurement system has already been devised within the scope of a project work. At the beginning, different concepts for leakage rate measurement were compared and tested for their suitability with regard to the requirements. Since the expected measuring range is of particular importance for the selection of a suitable concept, and there is currently no data on the leakage rates of REPAs, attempts to narrow down the measuring range had to be carried out first. (Hardelt, 2022)

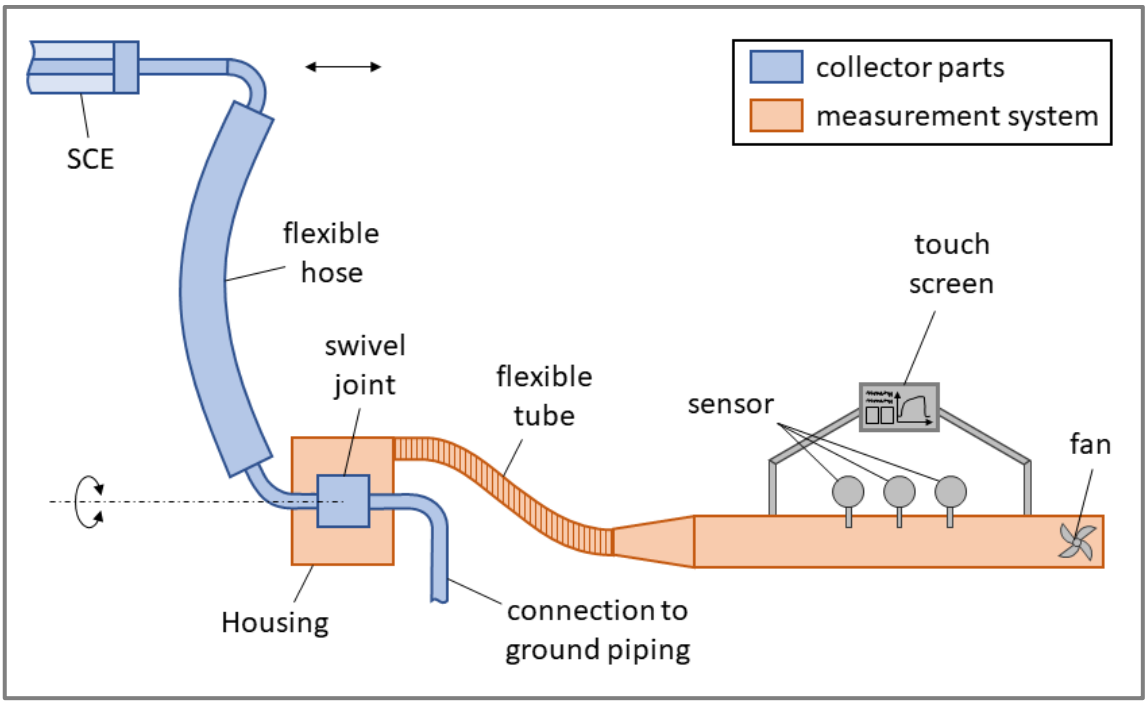

Figure 2.4, leakage rate measurement concept

The selected measurement concept, shown in Figure 2.4, is based on the concentration measurement of the gaseous HTF in a carrier air stream. For this purpose, a tube is equipped with a fan, generating a continuous air flow. A flexible tube connects the inlet of the tube to a housing, enclosing the swivel or ball joint to be examined. The fan creates a pressure drop in the system, drawing air into an inlet of the joint housing and mixing with the leaking HTF as it flows around the joint. Besides, sensors are integrated into the measuring section tube to determine the HTF concentration in the air stream and the mass flow of the total gas mixture. The measured values of the sensors are read out by a single-board computer (Raspberry Pi) and hence the leakage flow is calculated. (Hardelt, 2022, p. 21 ff.)

In order to be able to use the measurement system on the entire solar field independently of an external power supply, one challenge is to ensure small-sized sensors and actuators with an operation voltage of 12 V DC. In the search for possible components, no portable gas sensor calibrated for BP/DPO could be found. However, there is a variety of sensors with different measurement principles for the concentration determination of volatile organic compounds (VOC) (Szulczyński & Gębicki, 2017, p. 2 ff.). VOC definition is often given by the maximum vaporization temperature of 240 to 260 °C or the vapor pressure of at least 0.01 kPa (US EPA, 2014; NPI, 2009). In this case, the organic compound (OC) BP/DPO has an evaporation temperature of 257 °C and a vapor pressure of 0.001 kPa at 20 °C, thus being at the definition limit of VOC. Preliminary tests were

performed exposing the sensors to small BP/DPO concentrations and showed a response from both sensors. Initial tests already showed a response of both sensors to BP/DPO. However, strong fluctuations were observed, probably due the deposit of HTF on the pipe surfaces. Therefore, an evaluation of the measurement results was not possible. (Hardelt, 2022, p. 24 ff.)

2.5 Gas-wall interactions

When atoms or molecules of a gas phase (adsorptive) strike the surface of a solid (adsorbent), they are either repelled or remain attached to it. The forces applied by the particles of a substance per area of the adsorbent represent the partial pressure of the substance. The attached particles (adsorbate) are held to the adsorbent surface either by physical interactions (physisorption) or by electron exchange with the particles of the adsorbent (chemisorption). These processes, commonly called adsorption, are exothermic, so the adsorption energy E_{ad} is released when adsorption occurs. (Jousten, 2018, p. 265 ff.)

The inverse process, in which the adsorbate detaches from the surface and returns to the gas phase, is called desorption. For this process to happen, a desorption energy E_{des}, equal to E_{ad} is necessary. The energy required for the desorption of chemically adsorbed particles is about 10 times higher than that of physically adsorbed particles. (Jousten, 2018, p. 265 f.)

The adsorption rate indicates how many particles adsorb on the adsorbent over time and area. It is mainly dependent on the impingement rate, indicating the rate of hitting particles in a given time, and the adhesion probability. These in turn are dependent on the number of particles per volume and the average particle velocity of the adsorbate, and on the number of potential adsorption sites and the amount of already adsorbed particles on the adsorbent, respectively. On the other hand, an adsorbed particle desorbs as soon as its kinetic energy exceeds the desorption energy. The desorption rate is depending on the combination of adsorbent and adsorbate, and the kinetic energy of the particle, as a function of temperature. At constant pressure and temperature, the adsorption and desorption rates approach each other and thermodynamic equilibrium is reached. (Jousten, 2018, p. 52 f., 270 ff.)

Conversely, the term absorption is used when the adsorbed particles diffuse into the adsorbent and dissolve in it. Since a displacement energy must be applied for the changes in location to take place, diffusion is further enhanced at elevated temperatures. The terms adsorption and absorption can be summarized under sorption, considering

that the processes occur in parallel in many cases and the proportions cannot be clearly determined. The reverse process of absorption is known as outgassing. Compared to desorption, the outgassing process takes much longer because the dissolved particle has to diffuse back to the surface before desorbing. (Jousten, 2018, p. 266 f.)

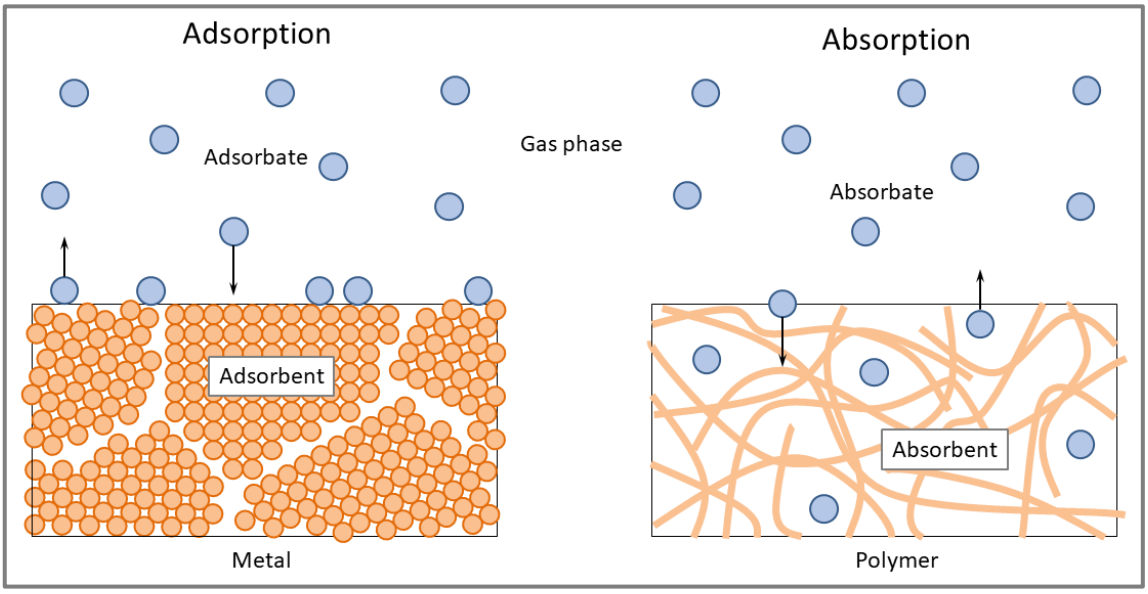

Figure 2.5, Sorption processes: adsorption (left), absorption (right)

The problem of sorption in gas mixtures flowing over a surface lies in the adsorbing particles that are removed from the gas phase and remain on the surface. This reduces the concentration of the adsorbate until an adsorption-desorption equilibrium is formed. If a subsequent gas mixture with a lower concentration flows along the surface, desorption will predominate, leading to an increasing concentration in the gas stream. For this reason, it is important to select suitable materials that have the lowest possible sorption tendency or to accelerate desorption processes by increasing the temperature. Typical materials used in the chemical industry for vessels, pipes or valves are stainless steels, polytetrafluoroethylene (PTFE or Teflon) and glass (Chan et al., 2022, p. 10575), due to their low reactivity and high chemical resistance. Nevertheless, sorption processes will occur with any pipe material (Matsunaga & Ziemann, 2010, p. 882).

Chan et al. (2022) studied the adsorption and desorption properties of these materials using a pharmaceutical ingredient as adsorbent at 24 °C. In this study, stainless steel showed higher adsorption and lower desorption than glass, indicating a higher affinity to the adsorbate. PTFE, unlike the other two materials, showed both higher adsorption and desorption with lower residual loading after flushing, which was attributed to the lower

coefficient of friction. However, looking at the driving variables of adsorption and desorption, this could also mean that the PTFE surface provides more adsorption sites but builds weaker bonds with the adsorbate.

In the case of Teflon and other hydrophobic surfaces, the experiments of Li et al. (1993, p. 580) showed that adsorption of various high-boiling substances represents only a negligible part of the sorption processes, being absorption predominant phenomenon. This was also observed by Matsunaga & Ziemann (2010) in their study on gas-wall partitioning of various OC in Teflon-coated vessels. They assumed that the OC particles permeate into the surface layers of the amorphous Teflon until further diffusion is prevented by the distortion of the polymer chains and the decreasing concentration, which is the driving force. The time constants to reach an equilibrium state in Matsunaga & Ziemann's experiments ranged from 8 to 60 minutes depending on the OC used. The ratio of absorbed particles to total introduced OC particles remained constant during multiple experiments with different gas concentrations, whereas a dependence on the ratio of the vessel volume to its surface area was described. With respect to the adsorption properties of different OCs, higher adsorption tendency was observed for substances with lower vapor pressure, which was also witnessed by Zhang et al. (2015, p. 4197) in their studies.

In addition to the effects of gas-wall partitioning on composition in static pressure vessels, the effects on the gas flowing through a pipe must as well be considered. Retention describes the process of setting the adsorption-desorption equilibrium in a pipe, affecting the concentration of the passing gas. Pagonis et al. (2017) studied the retention times for sampling OCs in Teflon tubes at room temperature. They found an almost proportional increase in the retention times with the length of the tube, as well as an almost inversely proportional relationship between the retention times and flow rate. Furthermore, the comparison of the tested OCs showed that there is an inversely proportional relationship between the vapor pressure of the adsorbate and the retention time. This also explains the positive effect of heating the tubing on the retention times, as the OCs also exhibit higher vapor pressures at elevated temperatures.

The adsorption properties of stainless steel lines were investigated by Derning et al. (2019) and Vaittinen et al. (2014) in comparative studies with other materials, including Teflon. The measurements of the latter study showed that the surface of SS316 stainless steel adsorbed 18 times the amount of NH3 molecules per centimeter than an equivalent surface of a PTFE tube. Increasing the temperature from 22 °C to 50 °C resulted in a decrease of the adsorbed molar quantity by about 20 %.

The experiments of Deming et al., in which stainless steel tubes made of SS304 were used, showed a retention time that was 20 times higher than in the case of PTFE tubes. It was noticeable that at the beginning the stainless-steel tubes did not allow any organic substances to pass through at all. In tests with a gas mixture of different OCs, it was found that after the initial period without detection, the substance with the higher vapor pressure was detected first and the measured values even exceeded the set concentration. At the time when the second substance could be measured, the measured value of the low-boiling substance settled at the expected value. The conclusion was that at the beginning of the tests the particles occupy the free adsorption sites on the tube surface. Once all the sites are taken, the substance with lower vapor pressure replaces the other substance due to higher binding forces. Experiments with a variation of the concentration of the OC used resulted in a strong decrease of the retention time until saturation of the stainless-steel tubes.

The difference between these materials lies in the driving mechanisms for gas-wall partitioning. Even though stainless steel is passivated by the inert chromium oxide layer on the surface compared to standard construction steel, it still has free electrons on the surface which cause relatively high binding energies (Harris et al., 2004, p. 2). Glass tubes, which were also studied by Deming et al. showed similar adsorption behavior to stainless steel tubes, but with a delay time lower by a factor of 2 (Deming et al., 2019, p. 3458). In conclusion, Teflon lines interfere significantly less with passing gas at low temperatures compared to glass or stainless steel. However, to further reduce the interference, it is reasonable to increase the temperature, which can significantly reduce the deposition of HTF caused by adsorption. Since absorption, which occurs mainly in Teflon lines, is enhanced by elevated temperatures, an analysis of the sorption properties of Teflon and stainless-steel at elevated temperatures is meaningful.

2.6 HTF concentration quantification

The measurement concept of leakage quantification presented in chapter 2.4 is based on the continuous measurement of the concentration of gaseous HTF in an air stream. Even though there are a variety of chemical sensors for different applications, the selection of a suitable one is not trivial. For example, wall interactions (even within sensors) can result in a severe delay in response to a change in concentration. In addition, measurement system requirements, such as portability, further limit the selection of suitable sensors.

Leidinger et al. (2014), Spinelle et al. (2017), Plass-Duelmer et al. (2017) and Szulczynski et al. (2017) investigated different portable sensors and their measurement principles in their studies and compared them with respect to the measurable substances and the measurement ranges. Although BP/DPO and its components were not mentioned in the studies nor in the data sheets of the sensors, a measurement range for the detection and quantification of benzene was given for most of them. The similar chemical structure of benzene C_6H_6, diphenyl oxide $(C_6H_5)_2O$ and biphenyl $(C_6H_5)_2$ led to the assumption that the sensors could also react to the constituents of BP/DPO. Finally, in the previous project work to this thesis, all these hypotheses have led to the comparison of six sensors and the selection of two potentially suitable sensors, considering the conditions of use and measurement requirements. (Hardelt, 2022, p. 24 ff.)

2.6.1 Dräger X-am 8000 Sensor

The *X-am 8000* sensor from *Dräger* is a battery-operated multi-gas detector suitable for the clearance measurement of gas containers and the monitoring of gas concentrations in the ambient air. By installing different sensors, the X-am 8000 can be adapted to the detection of various gases. For the measurement of hydrocarbons, two photo ionization detectors (PID) are available, covering different measuring ranges (the low concentration LC version of the sensor has been used here). The measured values of the sensor can be read on a display and exported to a computer after a series of measurements has been performed. (Dräger, 2020)

PID technology is based on the ionization of molecules of the substance to be measured. For this purpose, a UV lamp emits photons that ionize the molecules of the substance in a measuring chamber. Two electrodes in the measuring chamber are polarized and the flowing current is measured. This current depends on the number of ions as charge carriers and thus on the concentration of the substance to be measured. Even if the energy of the photons is not sufficient to ionize components of the air, all particles with an ionization energy below the photon energy are detected, making the sensor non-selective. (Spinelle et al., 2017, p. 3; Szulczyński & Gębicki, 2017, p. 7)

2.6.2 UniTec SENS-IT Benzene Sensor

The *SENS-IT Benzene* Sensor from *UniTec* is a compact gas sensor for monitoring the air quality and can be operated with 12 V DC. It contains a metal oxide semiconductor (MOS) measuring cell, being read out and processed in the embedded electronic board. The sensor can be accessed via an RS485 interface or an analog output. An internal storage of the data is not provided. (UniTec, 2022)

The measuring cell of the Sens-IT consists of a heated aluminum substrate of 2.5 * 2.5 mm² size, on which a semiconducting metal oxide is deposited. The type n semiconductor is heated to more than 200 °C, at which it chemically adsorbs oxygen from the ambient air. In the presence of a reducing gas such as benzene, the oxygen desorbs and reacts with the gas. Since the adsorption process of the oxygen is based on the transfer of free electrons from the semiconductor to the oxygen atom, this increases the resistance of the semiconductor. Accordingly, with increased gas concentration, the resistance decreases again. These values are measured by the sensor and converted to a concentration value with a calibration matrix of benzene. (UniTec, 2020)

Given that the reaction on the surface of the semiconductor can occur with any reducing gas, the sensor is non-selective. Thus, a reaction with BP/DPO is likely. In addition, the arrangement of the measuring cell, which is located directly at the air inlet of the sensor, and the heating of the sensor can prevent problems with gas-wall partitioning.

2.6.3 Sensor qualification tests

In order to investigate the suitability of the sensors for measuring BP/DPO concentrations in air, a test stand was set up as part of the previous project work (see Figure 2.6). The gas mixture was prepared in a stainless-steel cylinder. The pressure regulator and the fine-dosing valve were used to set a constant gas flow, which was monitored with the flow meter. An inlet for synthetic air was also provided for measuring reference values. Finally the corresponding sensor under investigation was connected at the outlet. (Hardelt, 2022, p. 27)

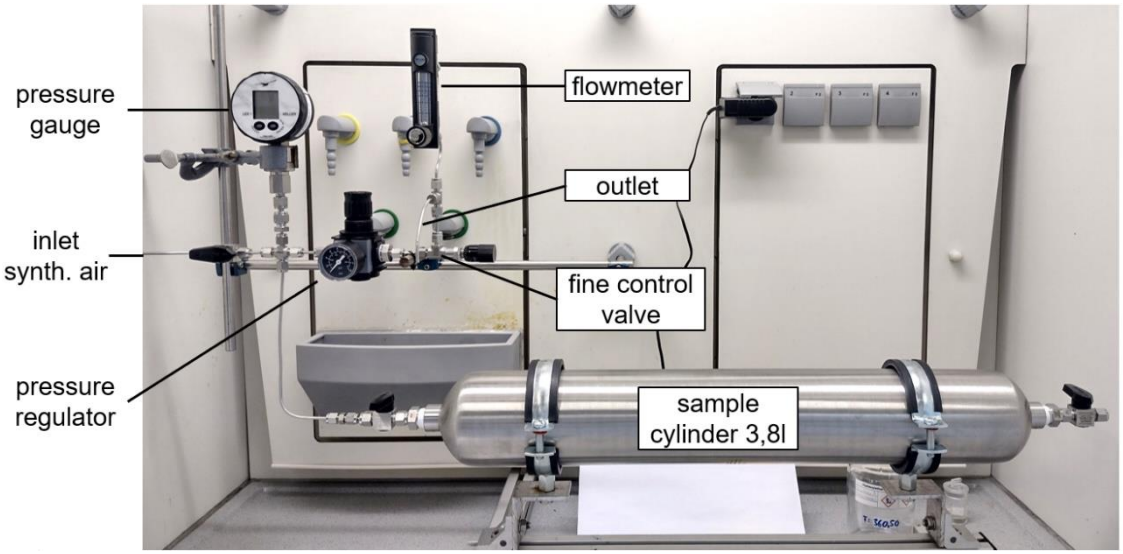

Figure 2.6, Test stand - project work

A reaction to the BP/DPO was detected by both sensors (PID and MOS). Subsequent tests with different concentrations were intended to narrow down the measuring range, but no repeatable results could be obtained by the sensors using this setup configuration. However, the cause of the deviations could relate to both the sensors and the test stand, which was not clarified within the scope of the project work.

2.6.4 Ultraviolet spectrophotometry

To curtail the aforementioned problem, the individual parts of the system, i.e. the sensor and the test setup, must be examined using qualified test methods. One possible approach is to use a calibrated laboratory instrument to examine the gas provided by the test stand and determine if it has the expected concentration. A UV spectrophotometer, is suitable for this purpose.

Ultraviolet spectroscopy is based on the phenomenon that the intensity I_0 of light drops to the intensity I when passing through an adsorbing sample. The correlation between the incident and attenuated power and the sample's properties is described in the Lambert-Beer law.

$$A = -\log T = \log \frac{I_0}{I} = \varepsilon \cdot b \cdot c \qquad \textit{Formula 2.1}$$

The absorbance A is a value for the optical density of the sample, the path length b is the distance the light travels in the sample and c is the concentration of the absorbing material. The molar absorptivity ε depends on both the wavelength of the light and the absorbing material and is also called the extinction coefficient. The ratio of the intensity of the emitted light I to the incident light intensity I_0 is called transmittance T. For a mixture of different absorbing substances, the individual absorptivities can be cumulated. (Skoog et al., 2017, p. 306)

In a UV spectrophotometer, a light beam is passed through the cuvette containing the substance to be detected. A wavelength selection device such as a monochromator is used to isolate the wavelength of interest from the emitted light and direct it to a detector. A detector measures the intensity of the light and converts this measured value into an electrical signal. By inserting the cuvette length and the molar absorptivity into the Lambert-Beer law, the concentration of the substance in the cuvette can then be calculated.

3 Objective

The present work is part of the development process a novel measurement system to quantify leakage rates of REPAs continuously under operating conditions. In a preceding project thesis, the requirements for the system were compiled and a concept designed. In the measurement system, the vaporous leakage is to be guided into a measurement section with a carrier air flow. Based on the mass flow of the gas mixture and the HTF concentration, the leakage rate can then be determined. For this purpose, a measurement method has to be selected and implemented to continuously quantify the HTF vapor in air.

3.1 Research question

The development of the measurement method includes the selection of a sensor that can quantify HTF vapor in air and the investigation of the conditions that allow good measurement results. This led to the following research question: Which portable sensor is suitable for the quantification of vaporous HTF in air, and under which operation conditions can it achieve good measurement accuracies in a leakage measurement system?

On the one hand, this includes the general qualification of the sensor with the recording of various values to characterize the sensor. In addition, the properties of the HTF must be investigated to understand the behavior of the gas mixture and the signal of the sensor. In order to find the most suitable operating conditions for the sensors, the properties of the gas mixture and the sensor behavior under different operating conditions must be investigated. Furthermore, sensors have to be tested under adequate conditions to verify their suitability for the measurement purpose.

3.2 Research procedure

In order to generate the gas mixture required for the tests and to be able to feed it into the sensors under variable operating conditions, a test rig will first be developed. It should be able to supply a constant volume flow with a defined HTF concentration and a defined output pressure for the entire duration of a test run. To ensure this, the system characteristics of this test rig are first investigated. This includes the true concentration provided to the sensor under test at the outlet of the test setup and the deviation from the set concentration. The delay in switching between the gas mixture and a reference gas, as well as the concentration curve observed during this process, are likewise important. Subsequently, the influence of the temperature as well as the tubing material on this system behavior is investigated.

A uniform test procedure is being developed for the qualification of the sensors, allowing conclusions to be drawn about the response and decay behavior of the sensor. The investigation of the relationship between the measured value of the sensor and the true concentration is of great importance here. These sensor characteristics are recorded under different gas concentrations in order to create a calibration curve from the data obtained. Furthermore, the measuring range of the sensor is narrowed down by varying the concentration.

As part of the work, the uncertainties caused by the measurement system and the experimental procedure and their effect on the measured values of the sensor are analyzed. This allows the calibration of the sensor to be evaluated and the measurement uncertainty of the sensor to be assessed.

Finally, a prototype is developed which conceptually corresponds to the measuring section of the designed leakage measurement system. This will be used to investigate the measurement behavior of the sensor under realistic conditions.

4 Experimental setup

This chapter describes the structural design of the test stand, followed by the variants of the physical design. The UV spectrophotometer, intended for the investigation of the sorption properties and for the qualification of the test rig, will be discussed in more detail. Thereafter, the general procedure of a series of experiments, consisting of several tests with constant conditions but decreasing concentrations, is explained. Finally, a summary is given of how the developed setup and the planned experimental procedure serve to answer the research question.

4.1 Test stand

The schematic structure of the test stand is shown in Figure 4.1. The core part of the experimental setup consists of a sample cylinder containing the gas mixture, a metering valve (MV_2) for flow regulation, the gas sensor, a pressure sensor and a flow meter for monitoring purposes. Since the cylinder needs to be dismantled for filling, it is equipped on both sides with a ball valve ($BV_{cyl,1}$ and $BV_{cyl,2}$) and a separation point towards the test setup. For zero-point measurements, a pressurized reference gas cylinder is connected to the gas sensor, by means of a regulating valve. A three-way valve enables quick switchover between the reference gas and the test gas. The piping can be cleaned either by flushing the test stand with reference gas through the BV_3 valve or by evacuating the contaminated area using the vacuum pump. The entire testing area is heated to examine the temperature effect on the system behavior.

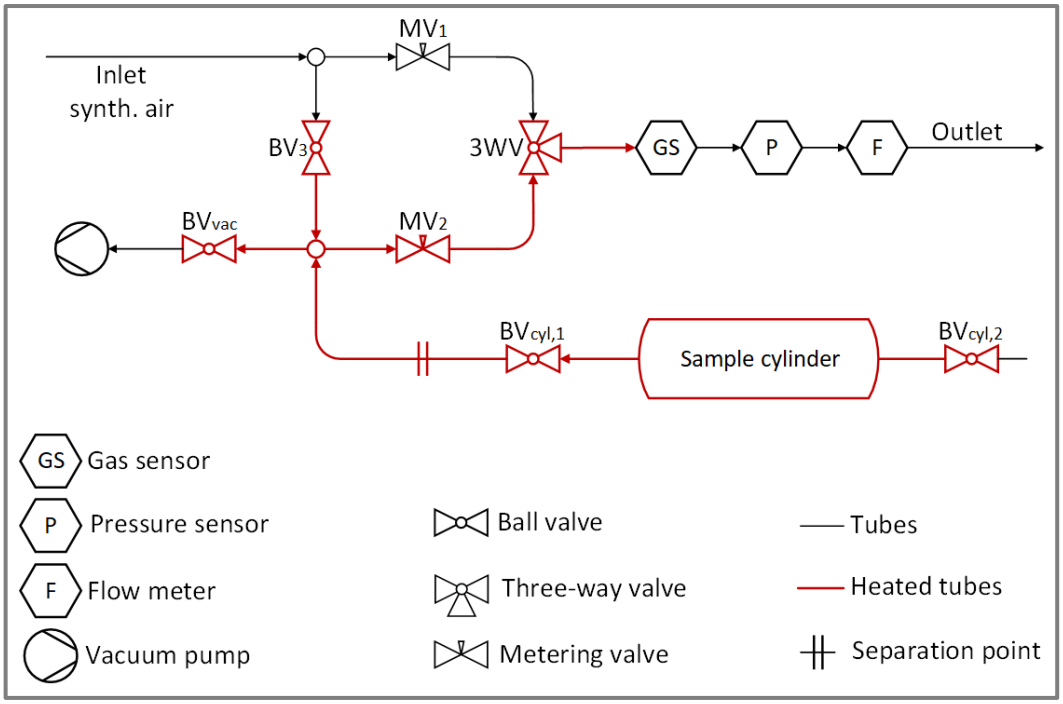

Figure 4.1, Test stand - schematic setup

In order to have a constant reference value for the tests and to exclude influences such as solvent vapors in the laboratory air or changing air humidity, synthetic air (80 % N2 and 20 % O2) is used as reference gas. This external gas supply can be used both to supply the sensors with the reference gas and to purge the system for cleaning purposes. Synthetic air was chosen because the SENS-IT requires oxygen for operation. The pressure provided by the compressed gas cylinder is reduced to a constant pressure of 4 bar due to operation reasons.

Figure 4.2 shows the final setup installed inside a fume hood. In the following, the individual components of the setup are described and their selection explained.

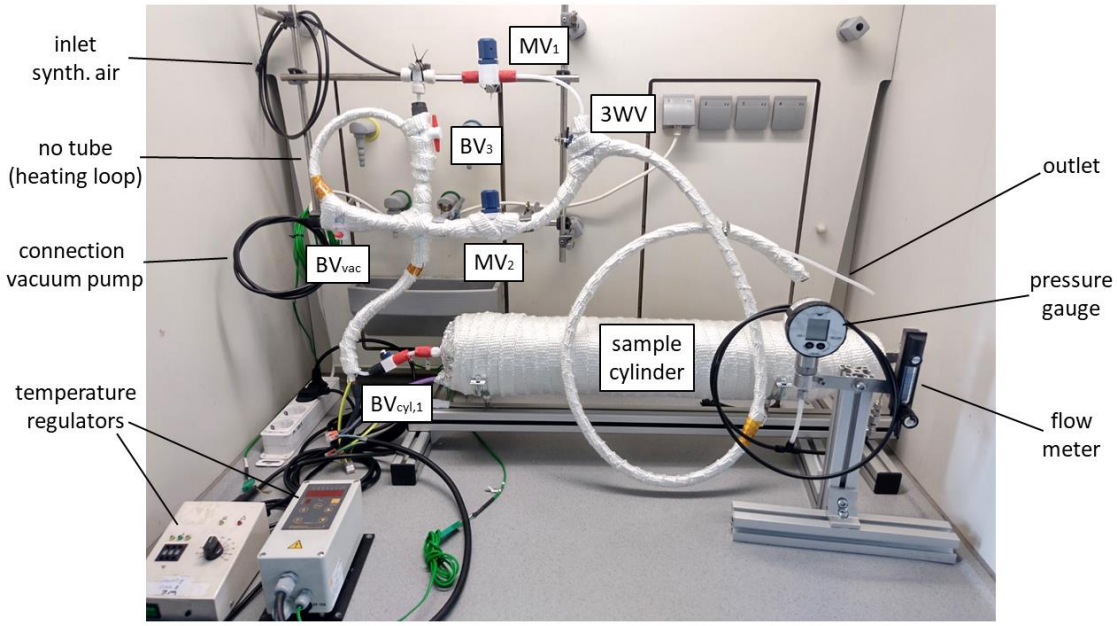

Figure 4.2, Test stand - final setup

The cylinder is made of stainless-steel SS 304 with PTFE coating. On both ends there is an opening with a threaded socket for connection of tubes or valves. The maximum operating temperature is 300 °C and the maximum permissible pressure is 100 bar. The volume is specified by the manufacturer as 3785 cm^3 with an uncertainty of ± 10 %. Since this value is used as a direct factor in the calculation of the gas concentration, this accuracy is insufficient. Therefore, the volume of 3701.8 ± 0.5 cm^3 between the valves on both sides of the cylinder was determined by the mass of insertable acetone. The contact surface area is approximately 1700 cm^2, calculated from dimensional data provided by the manufacturer (FITOK, 2022, p. 13). In the course of the experiment, an uncoated stainless-steel cylinder of the same design and base material is used as well for evaluating the influence of the material on the sorption characteristics of BP/DPO. The volume of this cylinder is 3800.9 ± 1.2 cm^3.

A laboratory screw joint system from Bola is used for the tubing assembly and instrumentation. The contact surfaces of the valves and fittings are made of polytetrafluoroethylene PTFE or polyphenylene sulfide PPS. The PTFE tubes for connecting the valves have an outer diameter of 6 mm and a wall thickness of 1 mm. The total tubing length, purged with the gas mixture during trials, is 2.2 m, giving a volume of 27.6 cm^3 and a surface area of 276.5 cm^2. The tubes are fixed and sealed with compression fittings. All line components have a temperature resistance of at least 200 °C and a pressure resistance of 6 bar.

The flow meter is a variable area flow meter with a measuring range of 0.1 to 1.2 l/min. It is required to set a constant flow rate via the metering valve. There is an additional metering valve on the inlet side of the flow meter, that is not used to control the gas flow, as this would expose the sensors to the cylinder pressure and change flow conditions. Instead, it is used to evacuate the system, enabling the entire contaminated line to be evacuated due to its positioning downstream of the gas sensor. In this context, the pressure gauge is used to detect leaks, since an increased pressure while evacuating can be an indication of a leak. Another reason for installing the pressure gauge and the flow meter downstream of the gas sensor is to avoid their influence on the gas mixture as both sensors have metallic surfaces and cannot be heated.

The entire area upstream of the sensor that comes into contact with the gas mixture is heated to investigate the temperature influence on the system behavior. In order to compensate for the large differences in the heat capacities of the hoses and valves compared to the cylinder, and also to allow easy removal of the cylinder, the heating is divided into two zones. On the one hand, the cylinder is spirally wrapped with two 250 W heating tapes to provide uniform heating. Several insulation layers improve the homogeneous temperature distribution and allow the cylinder to be transported in the hot state. On the other hand, the lines and valves are equipped with a heating tape parallel to the tubing that has a power of 90 W/m and can itself equalize the temperature differences between lines and valves by means of a temperature-dependent heating resistor. In addition, they are wrapped with aluminum foil for better temperature distribution and finally with fiberglass tape for insulation. Each zone has a controller with a thermocouple attached for actual value acquisition.

A rotary vane pump of the Vacuubrand RZ 2.5 type capable of achieving a final vacuum of $2 \cdot 10^{-3}$ mbar is used for evacuation. First and foremost, it serves for cleaning the inner piping area. In this case, evacuation of the tubes enhances desorption of BP/DPO from the tube walls, owing to its dependency on the partial pressure of HTF in the tube volume.

In contrast to purging the tube with reference gas, evacuation offers the advantage that dead ends can also be effectively cleaned. The second application is the evacuation of the inner area between the cylinder, MV_2, BV_3 and BV_{vac}, before the start of the experiment and its subsequent flooding with the gas mixture. This is done to prevent mixing with the air in the dead ends at the start of the test, prolonging the response of the test set-up.

4.1.1 UV-Vis spectrophotometer

To investigate the system behavior of the test rig, a gas measuring device is required with a calibration for the gas mixture, i.e. BP/DPO and synthetic air. The molar absorptivity of biphenyl and diphenyl oxide as a function of wavelength, can be found in the *National Institute of Standards and Technology* database (NIST, 2022; Almasy & Laemmel, 1950) and are used in this work. In Figure 4.3 the ultraviolet spectrum of the two substances in the range from 218 to 238 nm is plotted. In addition, using the approximated polynomials, the spectrum of a eutectic mixture of diphenyl ether (67.5 %) and biphenyl (23.5 %) was calculated and inserted into the diagram. Air does not show absorption in this wavelength range (Wiegleb, 2016, p. 479).

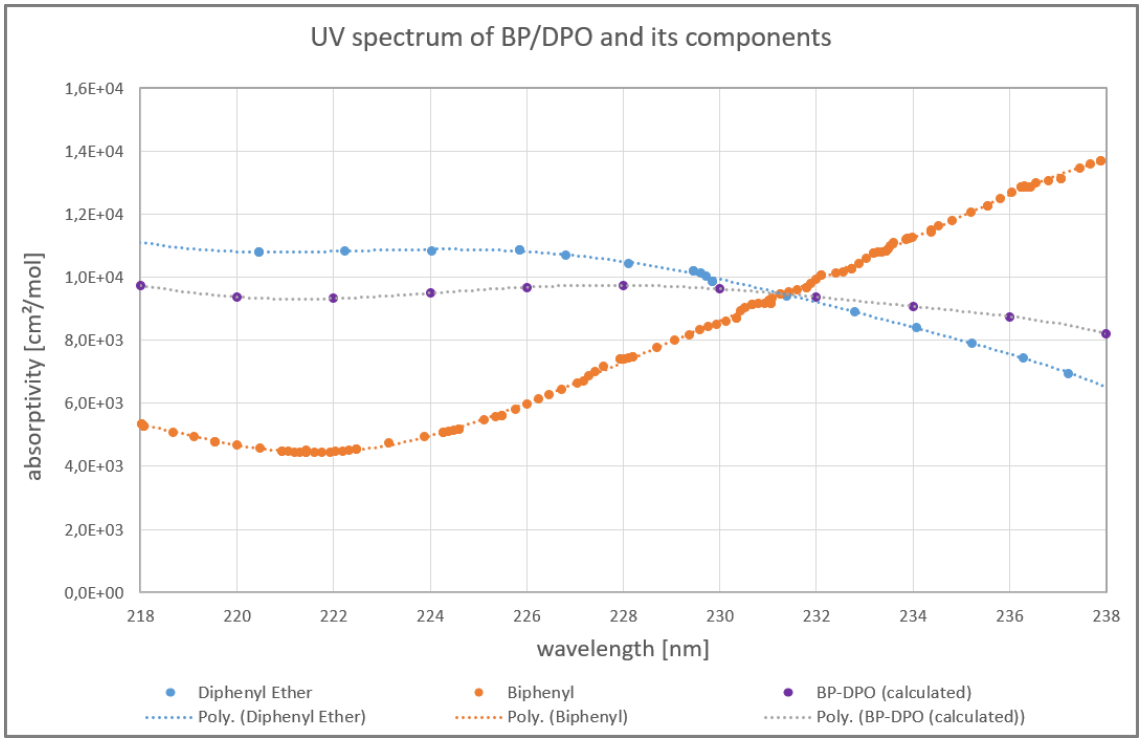

Figure 4.3, UV spectrum of BP/DPO and its components

The Cary 60 UV-Vis spectrophotometer from Agilent Technologies is used to investigate the system properties of the test stand. The gas mixture to be analyzed flows through a cylindrical cuvette made of quartz glass with a path length of 100 mm. It has a measured

volume of 30.13 cm^3 and a surface area of 62.5 cm^2. This 100 mm-long path was chosen because low absorbance values are expected for the low BP/DPO concentrations and this way the optimum absorption sensitivity is enabled. In addition, increasing the length of the cuvette reduces the relative errors of reflection losses, losses at the gas-wall and wall-gas transitions, and the influences of adsorption at the end walls. As shown in Figure 4.4, the cuvette is mounted in an aluminum cuvette holder with cooling/heating channels. By using a Jabulo CF31 thermostat with ethylene glycol as heat transfer medium, the cuvette can be heated up to 165 °C. A picture of the entire experimental setup with UV spectrophotometer and thermostat is included in Appendix A.

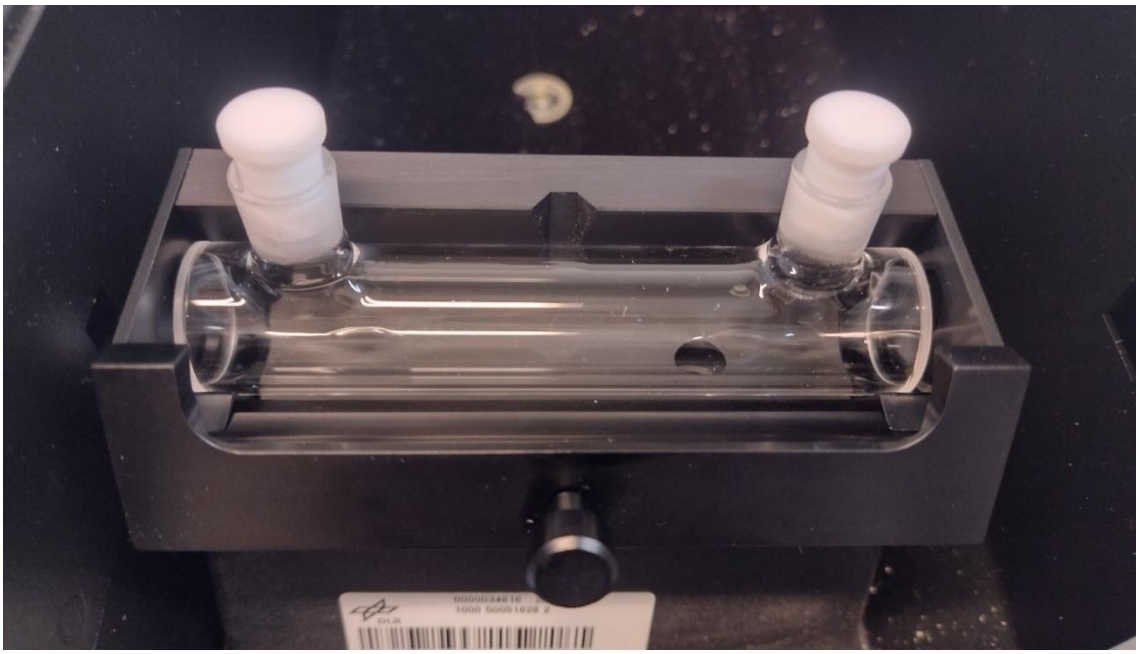

Figure 4.4, Cuvette in thermostatted aluminium holder

The Cary 60 has various measurement modes, including a scan over the wavelength range from 190 to 1100 nm and a kinetic program for determining the absorbance with a temporal resolution of 0.1 s. In both cases, the measurement is carried out in the same way. For the kinetic measurements, the wavelength 228 nm is selected because it corresponds to the maximum BP/DPO absorptivity in the previously calculated spectrum (Figure 4.3). In order to verify this, a scan measurement was carried out with BP/DPO vapor in the cuvette. For this purpose, first a reference measurement was made with air in the cuvette to record the baseline of the instrument. Then, a droplet of BP/DPO was applied on the bottom of one of the Teflon plugs and the cuvette was closed again. After an evaporation time of approximately one hour at 24 °C, the measurement was performed. The difference of the curves representing the absorbance of the BP/DPO vapor in the cuvette showed a spectrum similar to the calculated one.

4.2 Experimental procedure

The general procedure of a measurement series can be divided into three steps. The test preparation includes the production of the initial gas mixture as well as the preparation of the test setup. The test run includes the actual gas measurement as well as a zero-point measurement before and after the gas measurement. After each test run, the system is cleaned for the subsequent tests and the new gas mixture is prepared.

4.2.1 Initial cylinder filling

Since no supplier for calibration gas with BP/DPO could be found, the required mixtures are prepared by mixing synthetic air and HTF on site. Before filling with HTF, the cylinder is evacuated and heated to remove any residues from previous tests. It is then filled with synthetic air slightly above ambient pressure. The weight of a 2 µl syringe filled with liquid BP/DPO is measured subsequently. A Sartorius ME36S precision balance with a repeatability of $\pm \leq 2$ µg and a linearity of $\pm \leq 10$ µg is used for this purpose. The mass required for the experiment is applied to the tip of an approximately 10 cm long sample carrier made of the material of the cylinder and inserted into the cylinder. The sample carrier, shown in Figure 4.5, is used for better wiping of the HTF from the syringe as well as for improved evaporation of the HTF and is fixed at the inlet of the cylinder. Since the density of BP/DPO at 20 °C is 1.064 kg/l and there is always residue left on the syringe, the scale of the syringe can be used to estimate the amount of HTF. By weighing the syringe again, the mass of HTF actually injected can be determined precisely.

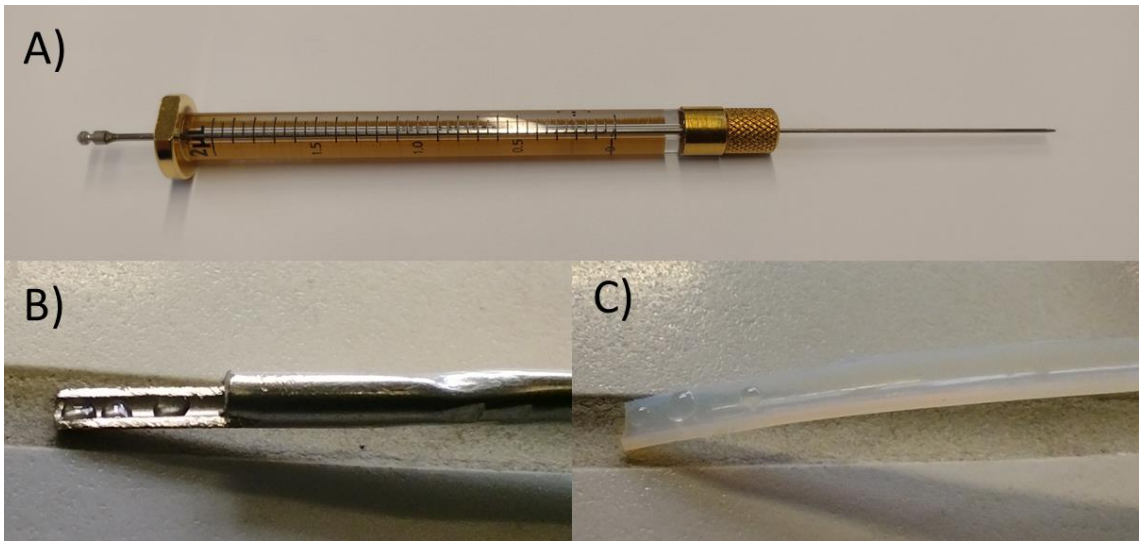

Figure 4.5, cylinder filling equipment: A) syringe; B) stainless steel sample carrier; C) PTFE sample carrier

The next step is to heat up the cylinder and hold it at the test temperature for one hour before pressurizing it with synthetic air to the starting pressure of 4 bar. The holding time

is necessary to allow the HTF to evaporate completely and prevent the pressure of the gas mixture from increasing further after pressurization. In addition, the synthetic air is fed into the cylinder at a low flow rate through heated lines to minimize an error in the concentration calculation due to incorrect gas temperatures. Pressure is measured by clamping the pressure sensor with an accuracy of 5 mbar to the port of the vacuum pump. Re-clamping is necessary because the cuvette is not designed for this pressure. After filling the air, an additional 10 minutes holding time is required to ensure uniform distribution of the HTF in the cylinder. The concentration of the gas mixture can now be determined using the following formula:

$$x = \frac{n_{HTF}}{n_{air} + n_{HTF}} = \frac{\frac{m_{HTF}}{M_{HTF}}}{\frac{p_{air} \cdot V}{R \cdot T} + \frac{m_{HTF}}{M_{HTF}}} \qquad \textit{Formula 4.1}$$

During the preparation of the cylinder, the UV spectrophotometer is taken into operation. In the case of the calibration experiments, where the measurement behavior of one of the portable gas sensors is investigated, the sensor is clamped between the outlet of the cuvette and the flow meter. This arrangement is chosen because any influence of the heated cuvette on the calibration gas is expected to be less than that of the portable sensors. The inserted sensor is started up as well. Throughout the further explanations, the case of a calibration experiment and thus the presence of a portable sensor will always be assumed. Since there is a frequent switching of the valves during the measurements, the gas lines operated during this process for synthetic air or the calibration gas are displayed again in Figure 4.6.

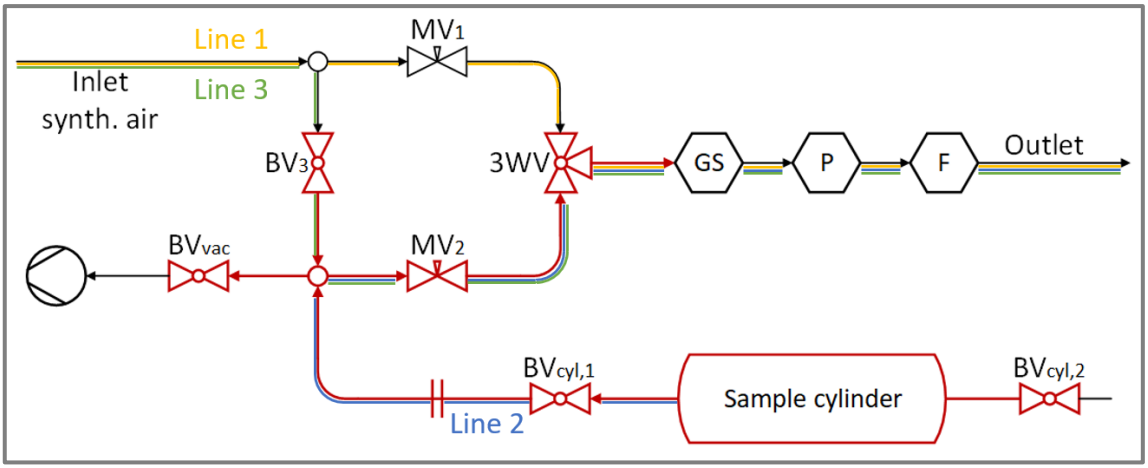

Figure 4.6, test stand - sample lines

Via line 1, the sensors are flushed with synthetic air prior to the start of the test to reach a constant value. As soon as the mixing time of the cylinder has expired, the outlet valve

of the cylinder is opened and the gas mixture is fed into the previously evacuated area between BV_{vac}, BV_3 and MV_2. At this point, the test run can be started.

4.2.2 Test run

The recording of the measured values takes 15 minutes and can be followed in Figure 4.7, showing an example measurement of the UV spectrophotometer. In the kinetics program of the UV spectrophotometer, this test duration can be predefined. The two portable sensors, on the other hand, record the concentration values permanently after start-up. Therefore, when starting the experiment, the kinetics program is triggered and the system time of the installed portable sensor is captured. In the first 60 seconds, synthetic air continues to be purged via line 1. The mean of the measured values from this time serves as the zero level and thus is the basis for calculating the concentration values of the sensors.

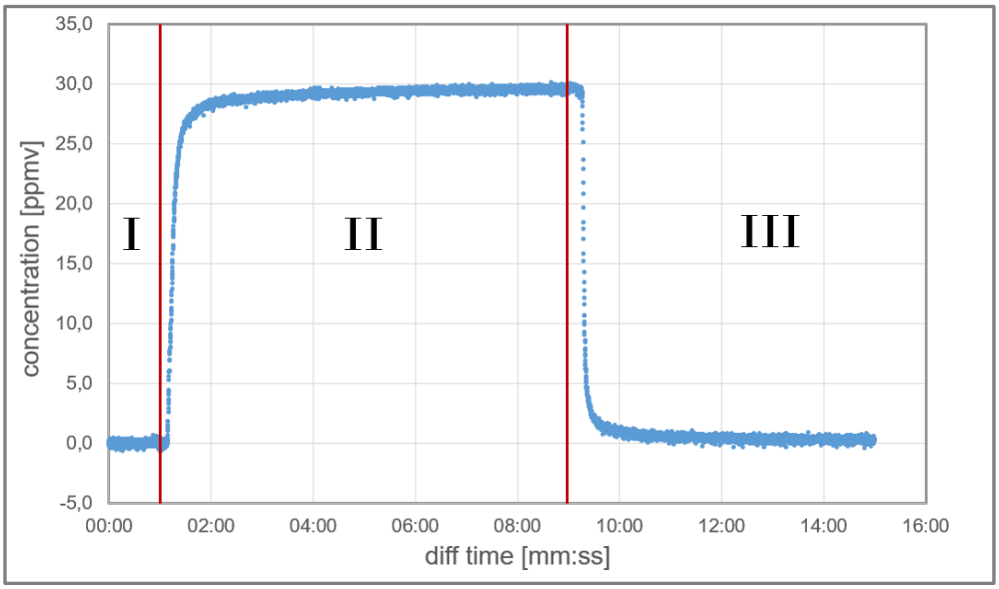

Figure 4.7, sequence of measuring run

Then the three-way valve 3WV is shifted and the fine dosing valve MV_2 is opened so that the calibration gas flows through the sensors via line 2. Since the fine dosing valves change their flow rate when exposed to high pressure on the outlet side, they cannot be set to the required flow rate until 3WV is switched to the corresponding line. Since the adjustment of the fine metering valves takes a few seconds, the time of opening is also recorded for the calculation of the response times of the sensors. In addition, the cylinder pressure and thus the inlet pressure of MV_2 continuously decreases during the experimental run, requiring MV_2 to be readjusted to ensure a constant gas flow in the sensors. The purging time with the calibration gas is limited to 8 minutes due to the cylinder volume and pressure of 4 bar. To calculate the achieved concentration, the mean of the last

30 seconds is calculated and the zero level is subtracted. After 8 minutes have elapsed, the system is switched back to purging with synthetic air. The time of opening of MV_1 is recorded and line 1 is flushed with constant air flow until the end of the test time in order to evaluate the decay time of the sensor.

4.2.3 Dilution and cleaning

After the test run, the cylinder still contains the gas mixture with the remaining pressure p_{rem}. In an ideal case with perfect mixing and without sorption processes, the HTF concentration of the mixture would still match the set concentration. This ideal case will be assumed in the further course. This allows to calculate the remaining amount of HTF using the remaining pressure and to generate a new gas mixture with a lower HTF concentration by repressuring with synthetic air. To prevent the HTF in the lines from being pushed back into the cylinder, the contaminated lines are evacuated beforehand.

The measurement of different concentrations is necessary to analyze the influence of the concentration on the system behavior, to determine the measuring range of the sensors and to obtain a calibration curve for the sensors. There are several reasons why the lower concentrations are not produced using the method presented in chapter 4.2.1. Firstly, the weighing process and the balance also have a particular uncertainty, which increases in relative terms as the concentration decreases. Secondly, the cleaning, weighing, heating and evaporation processes are very time-consuming. In contrast, the dilution method only requires waiting until the HTF is homogeneously distributed in the cylinder.

During this time, synthetic air continues to be supplied to the sensors via line 1 to restore their initial zero value. This also helps to clean the tubing between the 3WV and the UV spectrophotometer for the subsequent test. Simultaneously, the remaining tubing is cleaned by evacuation.

4.3 Summary

In this chapter, an experimental setup was designed to supply gas sensors with a calibration gas consisting of synthetic air and BP/DPO over a period of several minutes. In order to record a zero measurement, as well as sensor characteristics such as response and decay behavior, a switchable connection for pure synthetic air was additionally provided. The entire system can be heated up to 165 °C and the suitability of PTFE and stainless steel as construction materials with regard to their sorption properties can be investigated by replacing the cylinder.

With regard to the research question, the selected uniform experimental procedure enables the investigation of the sensors' characteristic behavior and the comparison of the influence of temperature and material to identify good operating conditions for the sensors. To ensure the suitability of the experimental setup, to investigate the performance of the system and to verify the measured values of the sensors directly, a UV spectrophotometer is used. This can be calibrated for the quantification of BP/DPO using literature values.

5 Design of experiments

In chapter 5, the tests that will be carried out with the test stand are planned. First, the framework conditions for the tests and the parameters that are to be kept constant during all tests are defined. Subsequently, an explanation is given of which tests are required to qualify the test rig and to analyze the temperature and material influences. The measurands which are to be determined from the tests and which serve the characteristic description of the test stand are specified. Finally, the experiments for the calibration of the sensors are explained and the aspects for the comparison of the sensors are described.

For each parameter set of temperature and material, serving the analysis of the influence of these parameters on sorption, at least three measurements with different concentrations are performed. The same applies to the measurements for calibration of the portable sensors. This allows an analysis of the linearity of the concentration influence. In addition, each of these series of measurements is performed three times. Since for each of these repetitions the gas mixture is prepared anew, a statement about the repeatability of the entire test sequence can be made based on the deviation of the tests with the same parameters from each other.

All test series are started with the filling of approx. 2 mg HTF and 4 bar synthetic air into the cylinder of 3.7 or 3.8 liters of volume. Since the HTF filling process has limited repeatability, there will be deviations in the starting concentration and thus in all further concentrations, but these will be accurately documented by weighing. The volume flow during the test run is set to 0.5 l/min both when purging with synthetic air and when using the test gas. On the one hand, this volume flow is high enough to supply the sensors with a sufficient gas mixture, and on the other hand, it is chosen that low in order to achieve the longest possible test duration.

5.1 Test stand qualification

Even though the test setup was designed with great care, the system behavior of the test stand is not predictable in its entirety. It can be assumed that an infinitely long test period with constant conditions would also result in a constant concentration value at the measuring point. However, since the test duration is limited, it is important to determine the dynamic behavior of the test stand in order to be able to distinguish between the influence of the test stand and the influence of the sensor on the measured value deviation during the subsequent qualification of the sensors.

The ratio x_r of the concentration x_{UV} measured by the UV spectrometer and the concentration x_{cyl} calculated from the filling data allows the determination of the sorption within the system. The mean value of the last 30 seconds before the cylinder valve was closed is taken as the measured concentration $x_{UV,max}$. Since the cylinders have a significantly larger surface area with approx. 1700 cm² than the lines with approx. 270 cm², the ratio x_r is mainly determined by the sorption in the cylinder.

The response and decay behavior of the measurements with the UV spectrophotometer should provide further information about the sorption properties of the test stand. Since there is a homogeneous gas mixture in the cylinder at the start of the test and a sorption equilibrium already exists here, the delays occurring here are mainly due to sorption processes in the lines. The UV spectrophotometer is very well suited for these measurements, since it responds to changes itself without any time lag and the volume of air in the cuvette (30 ml) can be displaced in 3.6 seconds at a flow rate of 0.5 l/min. As a quantitative value for the response behavior, the retention time t_{ret} is to be used, elapsing from the opening of the valve until 90% of the maximum measured concentration $x_{UV,max}$ is reached. To compare the decay behavior, the purge time t_{pur} is used, passing until the measured value corresponds to only 10 % of the measured concentration.

The tests are started with the PTFE coated cylinder. According to the literature research, increasing the temperature can lead to two phenomena that influence the sorption behavior in opposite ways. On the one hand, the binding forces between the Teflon and the gas particles are reduced and desorption is enhanced. On the other hand, at elevated temperatures, more HTF can be dissolved in the Teflon, promoting absorption. Since the relationship of these phenomena and the exact temperature dependence is not known, the investigations of the sorption properties of the experimental setup are carried out at 5 different temperatures between 50 °C and the maximum temperature of 165 °C.

In contrast, only adsorption occurs with metals, decreasing with increased temperatures. That is why the stainless-steel cylinder is tested only under the maximum temperature of the test stand of 165 °C. The tests to be performed for the test stand qualification are listed in the experimental plan in Table 5-1. The tests of a series will be indicated by the number of the test series, a dash and a ‘0’ for the initial concentration or the number of dilutions.

Table 5-1, Test series to investigate the influence of material and temperature on sorption

Number of test series	Material	Temperature
1 – 3	PTFE	50
4 – 6	PTFE	80
7 – 9	PTFE	110
10 – 12	PTFE	140
13 – 15	PTFE	165
16 – 18	SS	165

5.2 Sensor calibration

The portable sensors X-am 8000 and the SENS-IT benzene are to be qualified and calibrated for the measurement of BP/DPO vapors. This includes the determination of the measurement limits of the sensors, as well as the reaction to changes in the gas concentration. These characteristic values of the sensors are of great importance for the evaluation of their suitability for use in a leakage measurement system.

The sensor tests are carried out using the combination of cylinder material and temperature that showed the lowest sorption in the test stand qualification studies. The Dräger X-am 8000 is tested first, followed by the SENS-IT benzene. For both sensors, the procedure is identical, but the concentration has to be adapted to the measuring range. As far as possible, the measured values are compared with those of the UV spectrophotometer.

At the beginning, an experiment to narrow down the measuring range is started with the standard experimental conditions of approx. 2 mg HTF. By multiple dilution of the gas by a factor of 2, the upper and lower limits of the measuring range can now be determined. Subsequently, three identical test series are carried out, each with three HTF concentrations in the measuring range.

The most important value for the calibration of the sensors is the response factor f, indicating the ratio of the true concentration value to the measured value. If different response factors occur for the different concentrations, a calibration curve must be created. In addition to the response factor as a value for the static measured value deviation, the dynamic behavior of the sensors is also to be investigated. For this purpose, the response time t_{res} is calculated analogously to the retention time t_{ret} of the test stand and the decay time t_{dec} analogously to the purge time t_{pur}.

6 Data evaluation

Using the raw data of the experiments, useful information is generated in this chapter, allowing to draw conclusions from the experiments. It starts with the data from the setup qualification. An explanation is given of how the characteristic values of the test stand are calculated and what uncertainties result from the measuring instruments, the test execution and the calculations. The results of the test stand qualification will then be presented and the findings discussed. For the portable sensor calibration tests, likewise the calculations are explained and the results are presented. Based on these results, the suitability of the sensors for measurement application is investigated. Finally, the findings of this chapter are summarized and an explanation of how they serve to answer the research question is provided.

6.1 Presentation of data

In the context of the qualification studies of the test rig, findings are to be drawn from the differences between the calculated HTF concentration and the concentration measured with the UV spectrophotometer. However, since there are many different methods for quantifying the concentration of a substance in a mixture, whose values can differ greatly for the same mixture, a uniform unit must first be selected.

For gas sensors, the specification of the molar concentration c is common, which indicates the amount of substance of the specified component per volume. This specification is often used for sensors, since the physical measured value of the sensor, such as the absorbance in the case of the UV spectrometer, is often directly related to the molar concentration. However, since the molar concentration of gas mixtures is pressure-dependent, the gas mixture in the experimental setup can more effectively be characterized by the mole fraction x or the mass fraction w. These describe the ratio of the amount of substance or the mass of the specified component to the amount of substance or mass of the entire mixture. The conversion is carried out under the assumption of the validity of the ideal gas law by Formula 6.1.

$$x_1 = \frac{c_1}{\sum_{i=1}^{n} c_i} \qquad \textit{Formula 6.1}$$

6.1.1 Concentration calculation

To determine the mass m_{HTF} of the HTF filled into the cylinder, the weight of the syringe is measured before and after the HTF is deposited on the sample carrier. For statistical validation, three measurements are always performed and the mean value is calculated

(Formula 6.2). The difference between the mean values represents the mass of the HTF. Subsequently, the amount of substance n_{HTF} of the HTF can be determined by means of the molar mass M_{HTF} of the HTF (Formula 6.3).

$$m_{HTF} = \overline{m_0} - \overline{m_1} \qquad \textit{Formula 6.2}$$

$$n_{HTF} = \frac{m_{HTF}}{M_{HTF}} = \frac{m_{HTF}}{166\frac{g}{mol}} \qquad \textit{Formula 6.3}$$

After the synthetic air has been pressed on and the HTF has evaporated, the pressure p_{cyl} and the temperature T of the cylinder are measured. Now the amount of substance n_{air} of the synthetic air in the cylinder can be determined by the ideal gas law (Formula 6.4). Since the vapor pressure of 2 mg HTF at the highest set temperature of 165 °C is only 0.12 mbar, which is far below the accuracy of the pressure sensor of 5 mbar, the pressure of the synthetic air can be set equal to the pressure p_{cyl} of the cylinder. By substituting Formula 6.3 and Formula 6.4 into Formula 6.5, the molar fraction x_{HTF} can be calculated. Since the ratio of the amount of HTF used to the amount of synthetic air used in all tests is greater than or equal to 1:1000, a further simplification can be made by setting n_{tot} equal to n_{air}, thus obtaining Formula 6.6. This formula will be used further on to determine the molar fraction.

$$n_{air} = \frac{p_{cyl} \cdot V}{R \cdot T} = \frac{p_{cyl} \cdot V}{8.31446\frac{J}{mol \cdot K} \cdot T} \qquad \textit{Formula 6.4}$$

$$x_{cyl} = \frac{n_{HTF}}{n_{air} + n_{HTF}} = \frac{\frac{\overline{m_0} - \overline{m_1}}{M_{HTF}}}{\frac{p_{cyl} \cdot V}{R \cdot T} + \frac{\overline{m_0} - \overline{m_1}}{M_{HTF}}} \qquad \textit{Formula 6.5}$$

$$x_{cyl} = \frac{n_{HTF}}{n_{air}} = \frac{\frac{\overline{m_0} - \overline{m_1}}{M_{HTF}}}{\frac{p_{cyl} \cdot V}{R \cdot T}} \qquad \textit{Formula 6.6}$$

For the dilutions, it is assumed that the molar fraction of the HTF after performing the first experimental run is equal to the initial molar fraction. On the one hand, this assumes that the HTF is homogeneously distributed in the gas space. This can be accepted as correct, since the HTF was given sufficient time to mix with the air after evaporation.

Furthermore, the assumption presupposes the entire HTF to be in the gas phase and that no gas-wall partitioning occurs. Although this is not the case, further information on the sorption behavior can be generated by comparing the calculated values with the measured values of the UV spectrophotometer.

Given the constant temperature and the constant cylinder volume, the amount of HTF $n_{HTF,n}$ currently in the cylinder can be determined based on the amount of substance $n_{HTF,n-1}$ and the pressure $p_{cyl,n-1}$ measured before the last test run and the current pressure $p_{cyl,n}$ according to Formula 6.7. The new concentration after dilution is then calculated using Formula 6.6 again by inserting the new pressure.

$$n_{HTF,n} = n_{HTF,n-1} \cdot \frac{p_{cyl,n}}{p_{cyl,n-1}} \qquad \textit{Formula 6.7}$$

Table 6-1 shows the HTF concentrations of the calibration gases used for the tests to qualify the test rig. An increasing HTF content at elevated temperatures can be observed. This is due to the fact that the amount of HTF filled in and the starting pressure were kept constant, and the amount of material in the compressed air dropped as a result of the higher temperatures. However, this should not have a great influence on the evaluation, since an influence of the concentration can be analyzed via the dilution series.

Table 6-1, calibration HTF concentrations x_{cyl} calculated by filling conditions

parameter	Set 1	Set 2	Set 3
50 °C, PTFE	21.86 ppm	21.62 ppm	21.84 ppm
80 °C, PTFE	22.77 ppm	24.94 ppm	24.61 ppm
110 °C, PTFE	26.78 ppm	26.00 ppm	26.67 ppm
140 °C, PTFE	28.69 ppm	28.55 ppm	28.76 ppm
165 °C, PTFE	30.46 ppm	30.31 ppm	30.50 ppm
165 °C, SS	29.53 ppm	29.45 ppm	29.71 ppm

6.1.2 UV spectrophotometer

The UV spectrophotometer provides the absorbance as measured value, which is influenced by all intensity losses of the light beam from the lamp to the sensor. To isolate the absorbance of the gas sample A_{HTF} in the cuvette, the mean value of the absorbance of the first 60 seconds $\overline{A_0}$ is subtracted from the measured values A_{tot} (Formula 6.8).

$$A_{HTF}(t) = A_{tot}(t) - \overline{A_0} \qquad \textit{Formula 6.8}$$

The molar concentration is now determined using the Lambert Beer law (Formula 6.9) with the length of the cuvette l and the absorptivity ε determined in chapter 4.1.1.

$$c_{HTF} = \frac{A_{HTF}}{\varepsilon \cdot l} = \frac{A_{HTF}}{9746 \frac{cm^2}{mol} \cdot 10\ cm} = \frac{A_{HTF}}{97.46} \cdot \frac{mol}{l} \qquad \textit{Formula 6.9}$$

To compare the measured concentration with the calculated concentration, the molar concentration of the air must now be calculated according to the Formula 6.10 with the temperature and pressure inside the cuvette. The cell temperature is constantly controlled by the thermostat and the pressure is monitored by the pressure sensor downstream of the cuvette. By substituting Formula 6.9 and Formula 6.10 into Formula 6.11, the molar fraction x_{UV} can finally be determined.

$$c_{air} = \frac{n_{air}}{V} = \frac{p_{air}}{R \cdot T} = \frac{p_{air}}{8{,}31446 \frac{J}{K \cdot mol} \cdot T} \qquad \textit{Formula 6.10}$$

$$x_{UV} = \frac{c_{HTF}}{c_{air} + c_{HTF}} = \frac{\frac{A_{tot} - \overline{A_0}}{\varepsilon \cdot l}}{\frac{p_{air}}{R \cdot T} + \frac{A_{tot} - \overline{A_0}}{\varepsilon \cdot l}} \qquad \textit{Formula 6.11}$$

The UV spectrometer was set to measure absorbance at a sampling rate of f = 10 1/s. The molar fraction calculated from the measured values is plotted over time to further evaluate the concentration curve. Figure 6.1 shows the concentration curve for test 18-0, where each measuring point is shown as a blue dot. In addition, the parameters to be evaluated are plotted in this figure.

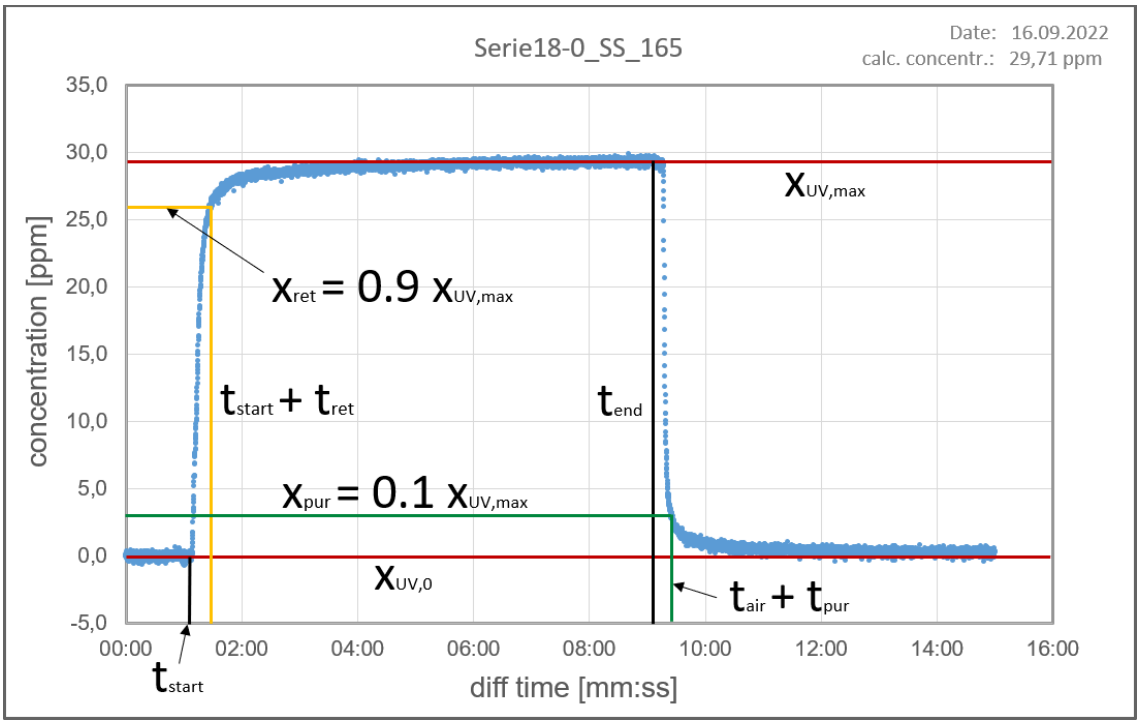

Figure 6.1, measurement analysis - UV spectrophotometer

At the beginning, the maximum measured concentration $x_{UV,max}$ is calculated as the mean value of the last 30 seconds before the end of flushing with HTF. The time t_{end} at which the three-way valve was flipped is taken from the experimental documentation. The ratio x_r of the measured concentration in the cuvette to the set concentration in the cylinder provides information about the residues of HTF in the system. Figure 6.2 shows the dependence of x_r on the cylinder material and the temperature of the experimental setup. Here, the crosses indicate the mean values from three repetitions performed and the error indicators represent the standard deviation.

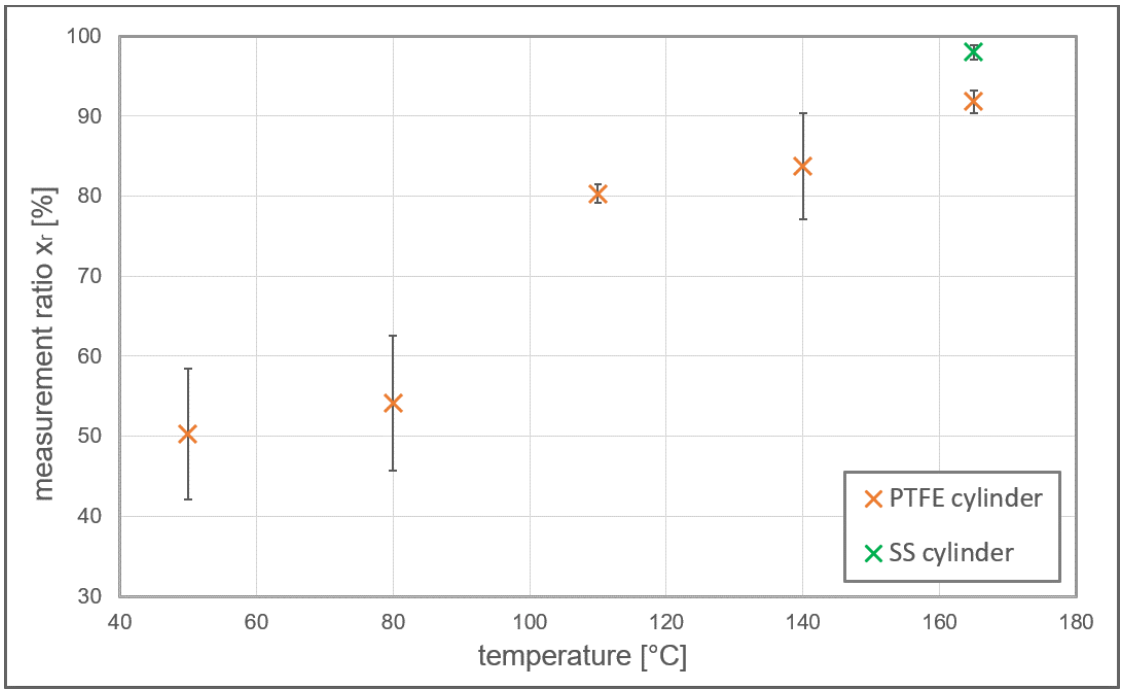

Figure 6.2, influence of cylinder material and temperature on the sorption properties

The diagram clearly shows the positive influence of the temperature increase on the reduction of the retained HTF. However, the fact that only 50% of the set concentration value could be measured in the tests at 50 °C and 80 °C can also be attributed to an incomplete evaporation of the HTF after the heating and homogenization time. With exception of the test at 140 °C, it can also be determined that higher temperature leads to better reproducibility of the tests. The comparison of the materials at 165 °C shows that the uncoated cylinder retains less HTF at this temperature. When the stainless-steel cylinder was used, a ratio of almost 100% was achieved, which would mean that no HTF remained in the cylinder.

The retention time t_{ret}, between opening the valve MV_2 and reaching 90 % of the maximum concentration $x_{UV,max}$, is determined graphically as shown in figure 6.1. Similarly, the purification time t_{pur} is determined by locating the intersection of the concentration curve with the concentration limit x_{pur}. The graphical evaluation was chosen for these values since the measured values of the UV spectrometer contain a certain basic noise and an evaluation based on exceeding or dropping below the critical values can lead to errors, especially in the case of flatter concentration curves and lower gas concentrations. In Figure 6.3, the determined times are plotted as a function of the cylinder material and the temperature.

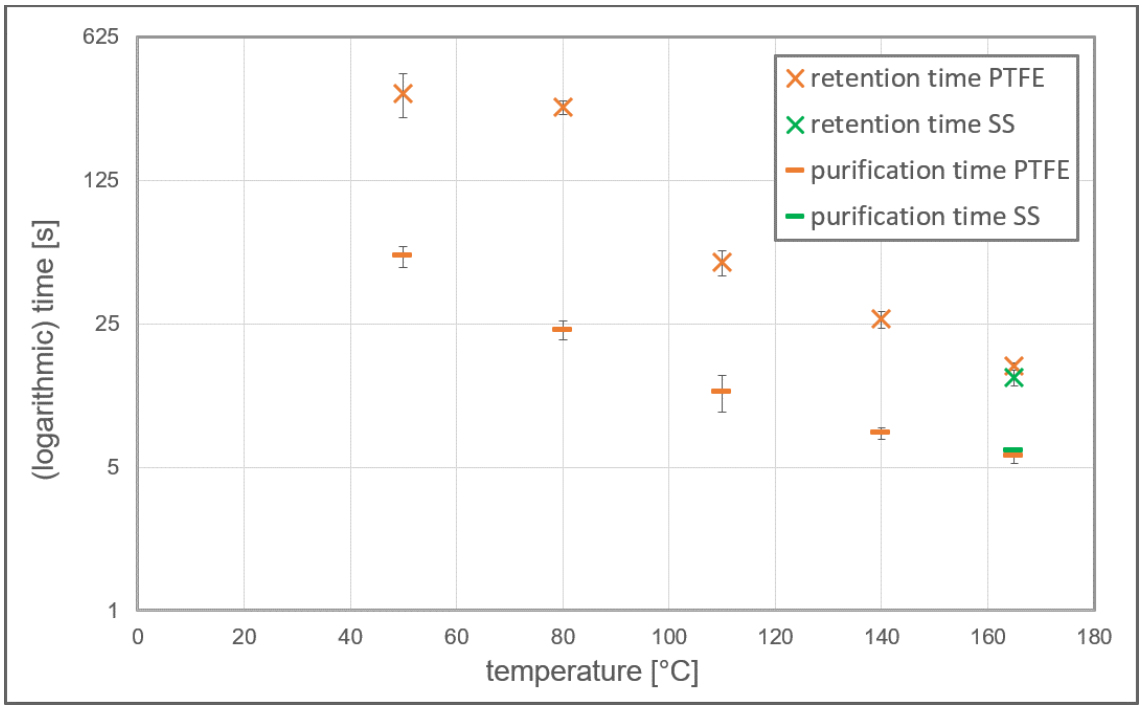

Figure 6.3, influence of material and temperature on retention and purification times

The diagram shows that the adjustment of the concentration to higher concentrations takes more time than the purification process. This could be due to the fact that gas wall partitioning also occurs in the tubes upstream of the three-way valve during the test start. In contrast, when switching to synthetic air, only the area from the three-way valve to the cuvette needs to be purged. Furthermore, the graph shows that both times decrease with increasing temperature. The comparison of the retention times of the PTFE cylinder with the uncoated cylinder at the same temperatures shows no significant difference.

6.2 Uncertainty assessment

The uncertainties of the calibration gas production and the concentration measurement using the UV spectrophotometer are based on the measurement uncertainties of the input quantities from Formula 6.6 and 6.11. To determine the total uncertainties of the concentration values, the measurement uncertainties of the input quantities must therefore first be determined. The uncertainties u_i of the influence quantities e_i can either be extracted from data sheets or calculated from the mean value $\bar{x}$ and the standard deviation s_x of n repeat measurements under constant conditions (Formula 6.12).

$$u = \frac{s}{\sqrt{n}} = \frac{1}{\sqrt{n}} \cdot \sqrt{\frac{1}{n-1} \cdot \sum_{j=1}^{n} (x_j - \bar{x})^2} \qquad \textit{Formula 6.12}$$

The influence of the uncertainty of the input quantity on the measurand $z(e_i)$ is determined by the correlation of the two quantities, which is defined in the corresponding formula for the calculation of z. This influence is therefore determined by the partial derivation of the formula according to the input quantity and multiplication of the term by the uncertainty of the input quantity (Formula 6.13). To determine the total uncertainty of the measurand z from the uncertainties of m independent input variables, Formula 6.14 is used (JCGM, 2008, p. 19).

$$u_{z,e,i} = \frac{\partial z}{\partial e_i} \cdot \Delta u_i \qquad \textit{Formula 6.13}$$

$$u_z = \sqrt{\sum_{i=1}^{m} \left(\frac{\partial z}{\partial e_i} \cdot \Delta u_i\right)^2} \qquad \textit{Formula 6.14}$$

6.2.1 Calibration gas uncertainty

The uncertainty of the concentration determination of the gas mixture by weighing the HTF is based on the measurement uncertainties of the variables influencing the mixture production. Derived from Formula 6.6, these include the uncertainties of weighing, temperature measurement, volume determination, pressure measurement and the molar mass of the HTF. The molar gas constant is accurately determined according to NIST (2019) and thus has no uncertainty. For the molar mass of the HTF, an uncertainty of $\pm$ 1 g/mol was assumed since no value for the uncertainty could be found. Since the determination of the HTF mass is a differential weighing, the uncertainty of the weighing results from the uncertainty of the balance as shown in Formula 6.15. The uncertainty of the temperature measurement and the pressure measurement could be taken directly from the data sheets of the sensors. For volume determination of the cylinders, the uncertainty was determined according to formula 6.12 from 5 measurement repetitions.

$$u_{m,HTF} = \sqrt{{u_{w,0}}^2 + {u_{w,1}}^2} = \sqrt{2 \cdot {u_{balance}}^2} \qquad \textit{Formula 6.15}$$

In Table 6-2, the uncertainties of the individual input variables on the gas production are listed using series 18 as an example. The determined initial concentration for measurement series 18, to which the uncertainties refer, is $x_{cyl} = 29.71\ \mathrm{ppm}$. The comparison of the deviations shows that the largest uncertainties come from the weighing itself and the

uncertainty of the molar mass. In contrast, the uncertainties due to errors in the pressure measurement or the volume determination are significantly smaller.

Table 6-2, influence of the input parameters on the uncertainty of the calibration gas

Uncertainty due to	Abs. deviation [ppm]	Rel. deviation [%]
HTF weighing	± 0.204	± 0.687
Molar mass of BP/DPO	± 0.179	± 0.602
Pressure measurement	± 0.037	± 0.125
Volume determination of the cylinder	± 0.019	± 0.063
Temperature measurement	± 0.102	± 0.342
Combined uncertainty	± 0.293	± 0.986

In the last line of Table 6-2, the combined standard uncertainty of the calibration gas is listed. However, this is not to be interpreted as the sum of the individual uncertainties, but instead must be calculated using Formula 6.16. This formula was created by inserting the uncertainties of the input quantities into Formula 6.14, allowing the uncertainty of the calibration gas production to be calculated for the individual tests.

$$u_{x,cyl} = \sqrt{\begin{matrix}\left(\frac{\partial x_{cyl}}{\partial m_{HTF}} \cdot u_{m,HTF}\right)^2 + \left(\frac{\partial x_{cyl}}{\partial M_{HTF}} \cdot u_{M,HTF}\right)^2 \\ + \left(\frac{\partial x_{cyl}}{\partial p_{cyl}} \cdot u_{p,cyl}\right)^2 + \left(\frac{\partial x_{cyl}}{\partial V_{cyl}} \cdot u_{V,cyl}\right)^2 \\ + \left(\frac{\partial x_{cyl}}{\partial T} \cdot u_T\right)^2\end{matrix}} \qquad \textit{Formula 6.16}$$

6.2.2 Dilution uncertainty

The uncertainty of a diluted gas mixture is calculated from the uncertainty of the initial mixture and the uncertainty of the pressure readings before and after pressurizing with synthetic air. Here, the uncertainty of the differential pressure measurement is given by the uncertainty of the pressure gauge multiplied by the factor $\sqrt{2}$ (using Formula 6.14). The standard uncertainty of the new gas mixture concentration can be calculated according to Formula 6.17.

$$u_{x,dil} = \sqrt{\left(\frac{\partial x_{dil}}{\partial x_{cyl,n-1}} \cdot u_{x,cyl,n-1}\right)^2 + \left(\frac{\partial x_{dil}}{\partial \Delta p} \cdot u_{\Delta p}\right)^2} \qquad \textit{Formula 6.17}$$

The absolute and relative uncertainties of the calibration gases from test series 18 are shown in Table 6-3. With dilutions by factor 2, a decrease in the absolute uncertainty and an increase in the relative uncertainty can be observed. In comparison with the two-step dilution between Test 18-0 and Test 18-2 resulting to a relative uncertainty of ± 1.404 %, a single dilution by a factor of 4 producing the same concentration would lead to a reduced relative uncertainty of 1.364 %. This procedure is not useful for the qualification of the test stand, since a three-stage measurement is to be performed here, but it can lead to lower uncertainties when calibrating the sensors at lower concentrations.

Table 6-3, Calibration gas uncertainties for test series 18

Test run	Concentration [ppm]	Abs. deviation ppm]	Rel. deviation [%]
Test 18-0	29.71	± 0.293	± 0.986
Test 18-1	14.85	± 0.180	± 1.213
Test 18-2	7.43	± 0.104	± 1.404

However, the calculated uncertainties only include the random scatter of the measured values relating to the input quantities. In addition, the gas wall partitioning inside the cylinder causes a higher molar fraction of the HTF in the cylinder after a test run than before the test run, since the exiting gas has a reduced concentration. This deviation of the concentration represents a systematic error that can be corrected. To do so, first a model describing the cause of the error under the test conditions would have to be set up. Using this model, a correction factor for the respective dilution could subsequently be determined. However, the present thesis is limited to finding the experimental parameters with the smallest systematic deviation.

6.2.3 UV-Spectrophotometer

The input quantities for the calculation of the HTF concentration c_{HTF} based on the measurements of the UV spectrophotometer using Lambert Beer's law (Formula 6.9) are the absorbance A_{HTF}, the molar absorbtivity ε and the path length l. Since the absorbance of the HTF is determined from the difference of the actual measured value A_{tot} and the basic synthetic air value $\overline{A_0}$, the uncertainty of the measured value is multiplied by $\sqrt{2}$ to obtain the uncertainty of A_{HTF} (Formula 6.14). The uncertainty of the path length l can be obtained from the data sheet of the cuvette.

The molar absorptivity ε for BP/DPO was determined from the molar absorbtivity coefficients of biphenyl and dipheny oxide and the fractions of the substances in the eutectic mixture as described in section 4.1.1. Regarding the molar absorptivity of diphenyl ether, weighted at 76.5 %, no uncertainty could be obtained from the literature. However, in the literature reference for the molar absorptivity of biphenyl, a relative uncertainty of 6 % is indicated (Almasy & Laemmel, 1950, p. 2095). This uncertainty is assumed as total uncertainty for the calculated absorptivity of BP/DPO due to the lack of further data.

Since the concentration value has so far been given in mol/l and the molar fraction (mol/mol) is required for comparison purposes, the uncertainties of the temperature and pressure in the cuvette, used for the conversion, must also be considered. For this purpose, the uncertainties of the thermostat and the pressure sensor can be obtained from the data sheets. The combined uncertainty $u_{x,UV}$ of the molar fraction of HTF determined by UV spectrophotometer can now be calculated by Formula 6.18.

$$u_{x,UV} = \sqrt{\begin{matrix}\left(\frac{\partial x_{UV}}{\partial \Delta A} \cdot u_{\Delta A}\right)^2 + \left(\frac{\partial x_{UV}}{\partial \varepsilon_{HTF}} \cdot u_{\varepsilon,HTF}\right)^2 \\ + \left(\frac{\partial x_{UV}}{\partial l} \cdot u_l\right)^2 + \left(\frac{\partial x_{UV}}{\partial p_{cuv}} \cdot u_{p,cuv}\right)^2 \\ + \left(\frac{\partial x_{UV}}{\partial T} \cdot u_T\right)^2\end{matrix}} \qquad \textit{Formula 6.18}$$

Table 6-4 lists the uncertainties of the maximum concentration measurement for Test 18-0. Both the individual uncertainties of the input quantities and the combined uncertainties are given as absolute and relative values. The measured value referred to by the relative uncertainties is $x_{UV} = 29.25\ \mathrm{ppm}$.

Table 6-4, influence of the input parameters on the uncertainty of the UV-spectrometric measurements

Uncertainty due to	Abs. deviation [ppm]	Rel. deviation [%]
Absorbance measurement	± 0.090	± 0.309
Molar absorptivity of BP/DPO	± 1.755	± 6.000
Cuvette path length	± 0.006	± 0.020
Pressure measurement	± 0.144	± 0.494
Temperature measurement	± 0.167	± 0.571
Combined uncertainty	± 1.771	± 6.055

The table shows that the uncertainty of the UV spectrometer measurements is primarily caused by the uncertainty of the molar absorptivity coefficient. Without the influence of the absorptivity coefficient, the combined uncertainty of the measurements from Test 18-0 would be just 0.239 ppm and 0.815%, respectively. However, since molar absorptivity is a constant value, a deviation of this value from the real molar absorptivity of BP/DPO will only result in a constant percentage deviation, which will not affect an assessment of the repeatability of tests or the analysis of the dynamic behavior of the test stand.

On the other hand, the measured value shows a certain background noise, arising directly from the measurement of the absorbance. This noise can be caused by uncontrolled variations in the gas properties, by external influences or directly by the measuring instrument used. Since it has a standard deviation of about ±0.2 ppm, the noise does not offer a great disturbance for the measurement of concentrations above 5 ppm. For the measurement of lower concentrations or the analysis of temporal developments with flat gradients, however, it poses a large uncertainty.

6.3 Discussion of the results

The expected strong influences of temperature and cylinder material on sorption were confirmed by the measurements for qualification of the test stand. Figure 6.4 shows the measurement ratios x_r of all the tests carried out. The mean values for tests with identical parameters have been calculated in order to maintain clarity.

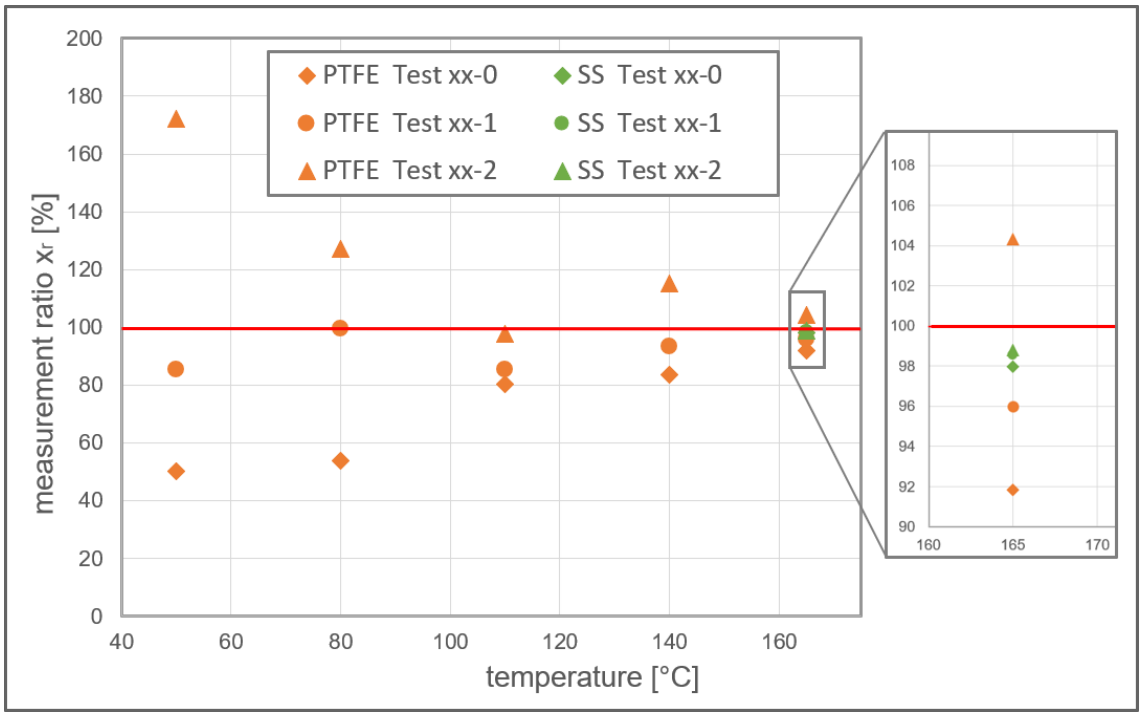

Figure 6.4, influence of cylinder material, temperature and HTF concentration on the sorption properties

With regard to the x_r ratios, an approximation of the measured values to the set concentrations in the cylinder can be seen with the increase in temperature for the Teflon cylinder. It is particularly noticeable that in the first tests (test xx-0) of a test series with the high initial HTF concentration of approx. 30 ppm, the measured values are significantly below the expected value. This may be due to the fact that the time for evaporation was not sufficient, or that the concentration of the gas mixture was significantly lowered due to gas-wall partitioning. In each of the second tests, the measured values and the set concentrations match quite well, and in the third tests (Test xx-2), the measured concentration is higher than the expected concentration of approx. 7.5 ppm in the cylinder. This is due to the desorption of HTF as the concentration in the cylinder decreases. This phenomenon can be observed with the Teflon cylinder even in the experiments at 165 °C on a small scale. However, the measurements with the stainless-steel cylinder are much closer. To examine them in greater detail, the measurement ratios of the experiments at 165 °C have been plotted against cylinder concentration in Figure 6.5.

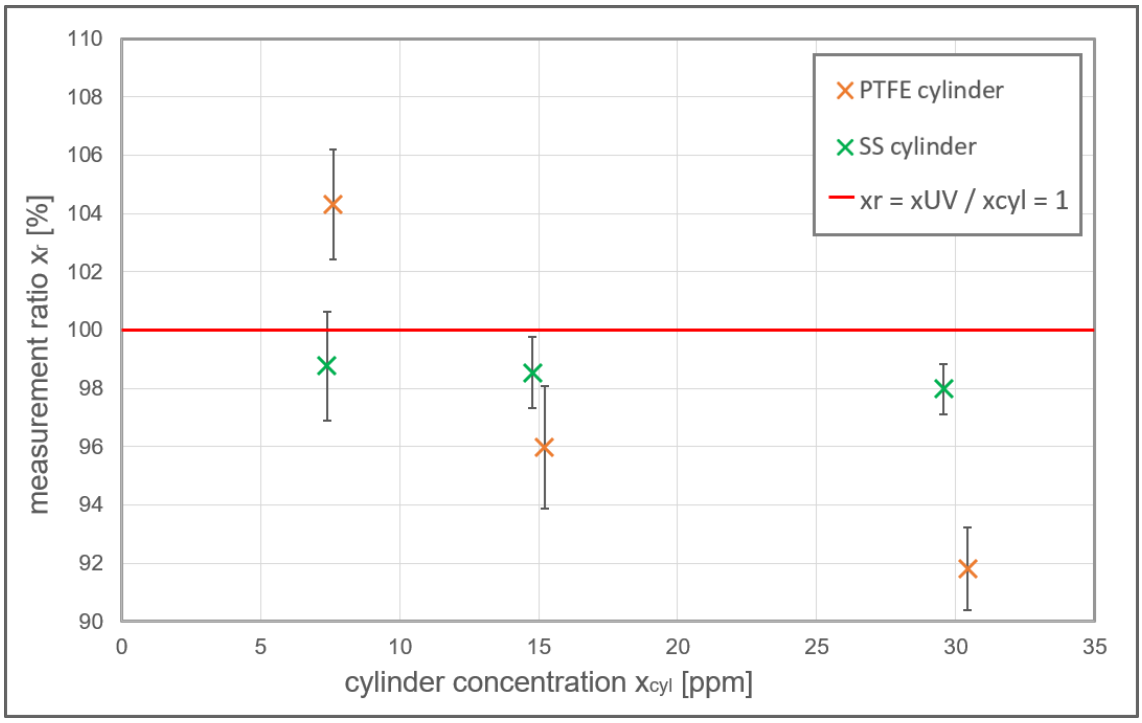

Figure 6.5, influence of concentration on the sorption properties

In addition to the increase in the x_r value towards lower concentrations, the tests with the coated cylinder also show a higher standard deviation, which is represented by the error indicators. In contrast, the measured values of the steel cylinder are almost constant over the entire concentration range. This means that lower concentrations can be produced by multiple dilution without large uncertainties. Due to the high uncertainty and noise in the measurements of the UV spectrophotometer, the low concentrations can no

longer be quantified by the UV spectrophotometer. This is especially important for the qualification of the sensors, since the selected sensors are expected to have a lower detection range than the UV spectrophotometer.

The high importance of the test stand sorption properties for the performed measurements is due to the limited test duration of 8 minutes and the requirement to achieve a stable value within this time. In comparison, the leakage of REPAs is typically not limited in time and does not show very dynamic properties. This is particularly the case for a measurement in the field, where the rotation of the joint is distributed over a whole day. However, in order to be able to determine a dependence of the leakage values on the rotation angle in the REPA test rig, in which a daily cycle is simulated in 3 minutes, the dynamic behavior of the measurement system is important.

6.4 Sensor qualification

The X-am 8000 and SENS-IT Benzene sensors are installed in the test stand one after the other and examined for qualification and calibration. Before starting the calibration tests, test measurements are carried out to investigate the general behavior of the sensor and to determine the upper measuring limit of the sensor for BP/DPO.

6.4.1 Dräger X-am 8000

The X-am 8000 with the LC-PID sensor has a measuring range of 0.05 ppm to 8 ppm for isobutene. It features a concentration resolution of 0.01 ppm and a sampling rate of 1/s. Figure 6.6 shows the sensor, which can be connected to the outlet of the cuvette with the inlet tube, depicted on the left side of the picture. Another tube was attached to the outlet side of the sensor and connected to the pressure and flow sensor to continue monitoring the volume flow.

Figure 6.6, Dräger X-am 8000 sensor

Since the sensor has an internal diaphragm pump and interrupts or even stops the measurement with an error message if the pump speed is incorrect, care must be taken to ensure a steady volume flow by accurately setting the regulating valve of the test stand. One of the preliminary measurements to investigate the sensor behavior is shown in Figure 6.7.

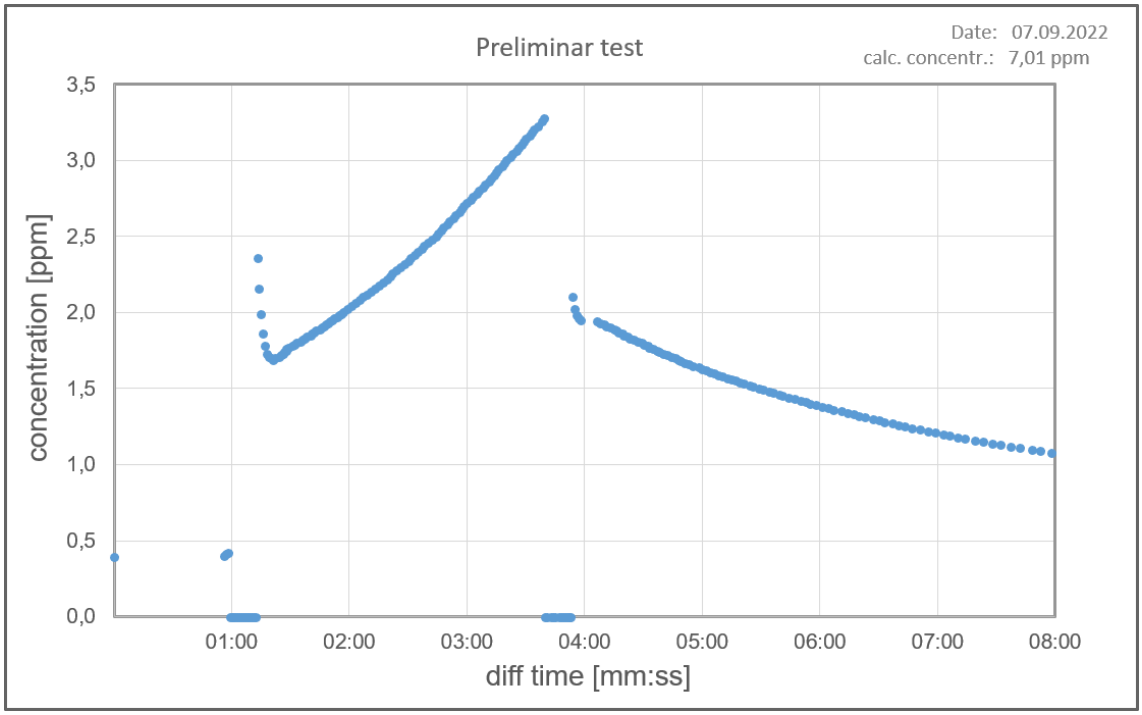

Figure 6.7, preliminary test - X-am 8000

Some observations can already be made on the basis of the concentration curve. For example, in the first minute before the start of the experiment, a gap can be seen in the measured values. The reason for this is that the X-am 8000 only records the measured values if they differ from the previous one. Since the sensor previously measured a constant concentration, no measured values are present here. At the same time, it can be seen that this constant reading, which was achieved by flushing with synthetic air, is at 0.4 ppm and not 0 ppm as expected, which will be discussed in more detail in the evaluation of the calibration tests. The fact that the concentration value briefly drops to 0 ppm before and after the test runs arises as a result of the change between calibration gas and synthetic air. The resulting short interruption of the volume flow leads to an error of the sensor which does not measure any concentration.

When purging with calibration gas, an almost constant increase of the measured value from 1.7 to 3.3 ppm can be seen over the test duration of 3 min. The UV spectrometer, which was operated at the same time, recorded an almost constant concentration value with a mean value of 7.09 ppm during the entire test period. The drop in the concentration

value when flushing with synthetic air starting at minute 4 is fairly flat and approaches the zero value rather slowly. In contrast, a purification time of 12 s was observed with the UV spectrophotometer.

For calibration, 3 test series were carried out with a starting concentration of approx. 10 ppm and dilution factors of 2. Before starting each test run, a constant value was reached. Subsequently, the test was carried out as described in section 4.2.2. Figure 6.8 shows the results of the tests with regard to the ratio of the measured concentration versus the concentration in the cylinder.

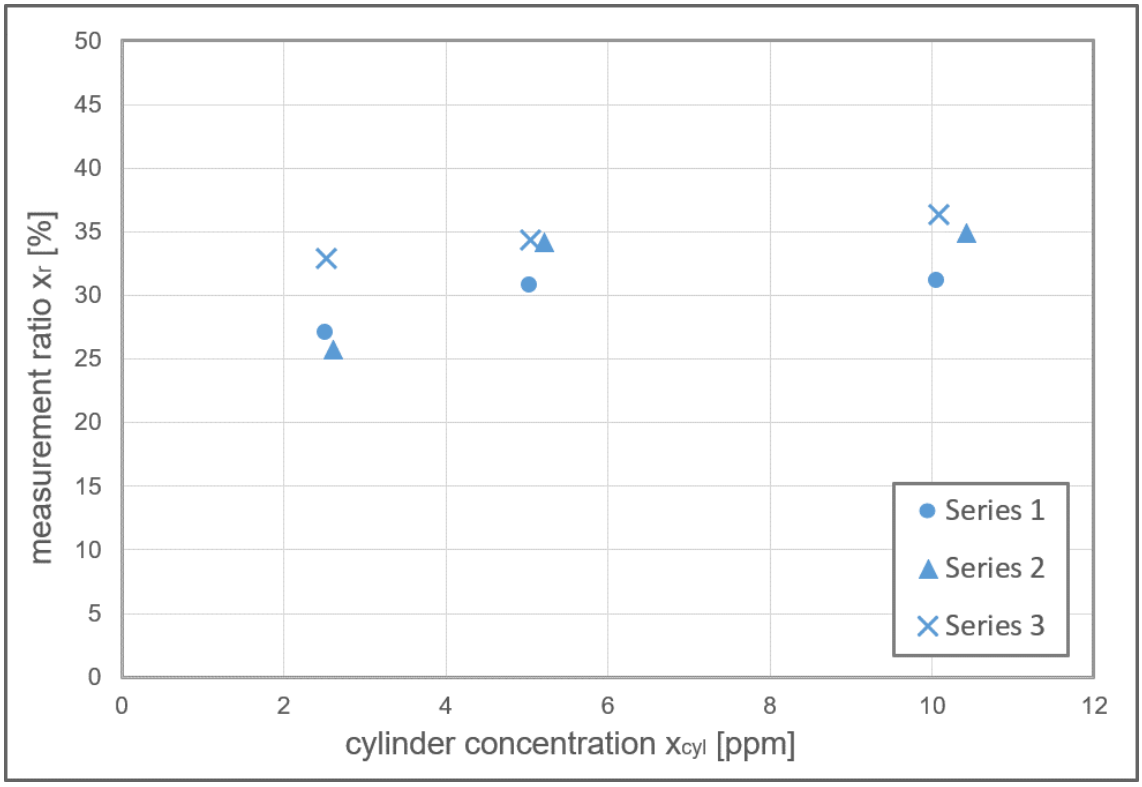

Figure 6.8, sensor qualification tests – Dräger X-am 8000

The measurement ratios from the experiments range between 25.7 and 36.3 % and on average show a slight increase at higher temperatures. However, since the course of the measured concentration increased in all tests until the end, it is not possible to conclude a response factor from the measured values and a calibration is therefore not possible.

The determination of the response time was not possible either, since a constant measured value was not achieved in any of the tests. With regard to the decay times, however, it can be said that when the sensor was flushed with synthetic air after the tests, it took between 20 and 120 minutes until a constant 0 value was reached again.

The inert response of the sensor can be due to various causes. On the one hand, normal sorption processes in the sensor or the supply tube can change the concentration of the gas mixture. Since the sensor cannot be heated, this cannot be counteracted. The sudden drop in gas temperature can also lead to condensation of HTF, which is then also deposited on the flowed surfaces. However, this phenomenon is expected to be highly concentration dependent. A third possible cause is that the PID measuring cell itself is very inert or contaminated. This could also explain the offset of the zero value, which varied slightly between experiments. The actual reason for the sluggish responses of the sensor is not analyzed in this paper. However, it should be noted that under these circumstances, the sensor is not suitable for the quantification of HTF vapors with dynamic concentration response.

6.4.2 UniTec SENS-IT Benzene

The SENS-IT Benzene (Figure 6.9) is calibrated for the measurement of benzene and has a measuring range of 0.1 to 30 ppb. The resolution is 0.1 ppb and the precision is 0.2 ppb. It records the measured value with a sample rate of 1/s. Since the sensor is actually intended for live monitoring of air quality in outdoor areas, it does not have a pump or a hose connection like the Dräger X-am 8000 does, but has a large opening at the top of the housing (left in the picture) and a ventilation opening at the bottom (right in the picture). For this reason, two adapters (white and black) were made to attach a hose to the inlet and outlet. In addition, several joints of the housing had to be sealed so that a measurement of the volume flow behind the sensor was possible.

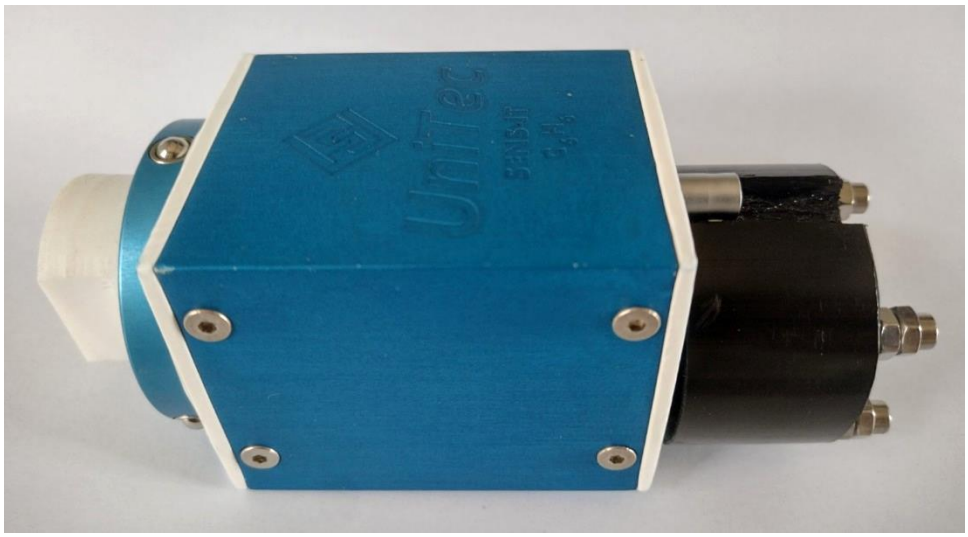

Figure 6.9, UniTec SENS-IT Benzene sensor

For the operation of the sensor, a computer is always required, which reads out the measured values of the sensor via an RS485 interface. For this purpose, a Python

program was created, which records the measured values, displays the current concentration value and saves the measured values in a .csv file.

In order to narrow down the measuring range, a preliminary measurement was also carried out with the SENS-IT at a gas concentration of 750 ppb, as shown in Figure 6.10. The measured value increases sharply at first when the valve is opened at minute 1:13, then flattens out during the course of the test, but does not reach a stable end value during the 8 minutes of the test. Switching from the calibration gas to the synthetic air first results in a short interruption of the flow and then leads to a sharp increase in the measured value at minute 9:16. After opening the dosing valve MV1, the measured value drops to 0 ppb within 70 s.

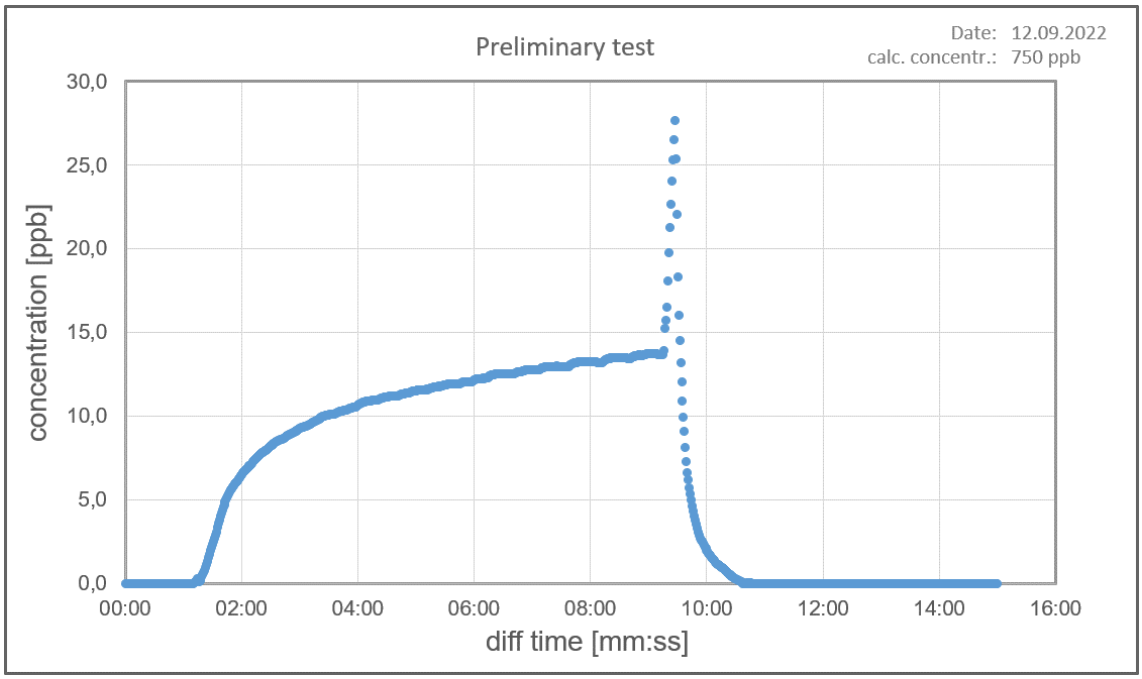

Figure 6.10, SENS-IT - preliminary test

For calibration, 3 test series were carried out. The first one had an initial concentration of 1.0 ppm and was diluted twice by a factor of 2. Test series 2 and 3, on the other hand, were performed with an initial concentration of 1.5 ppm and 3 dilutions by a factor of 2. Before the start of each test run, the sensor was purged with synthetic air to assume a value of 0 ppb. The test was then performed as described in Section 4.2.2. Figure 6.11 shows the results of the tests in terms of the relationship between the measurement ratio and the concentration in the cylinder. The trend lines were inserted only for better assignment of the individual measurements to the test series.

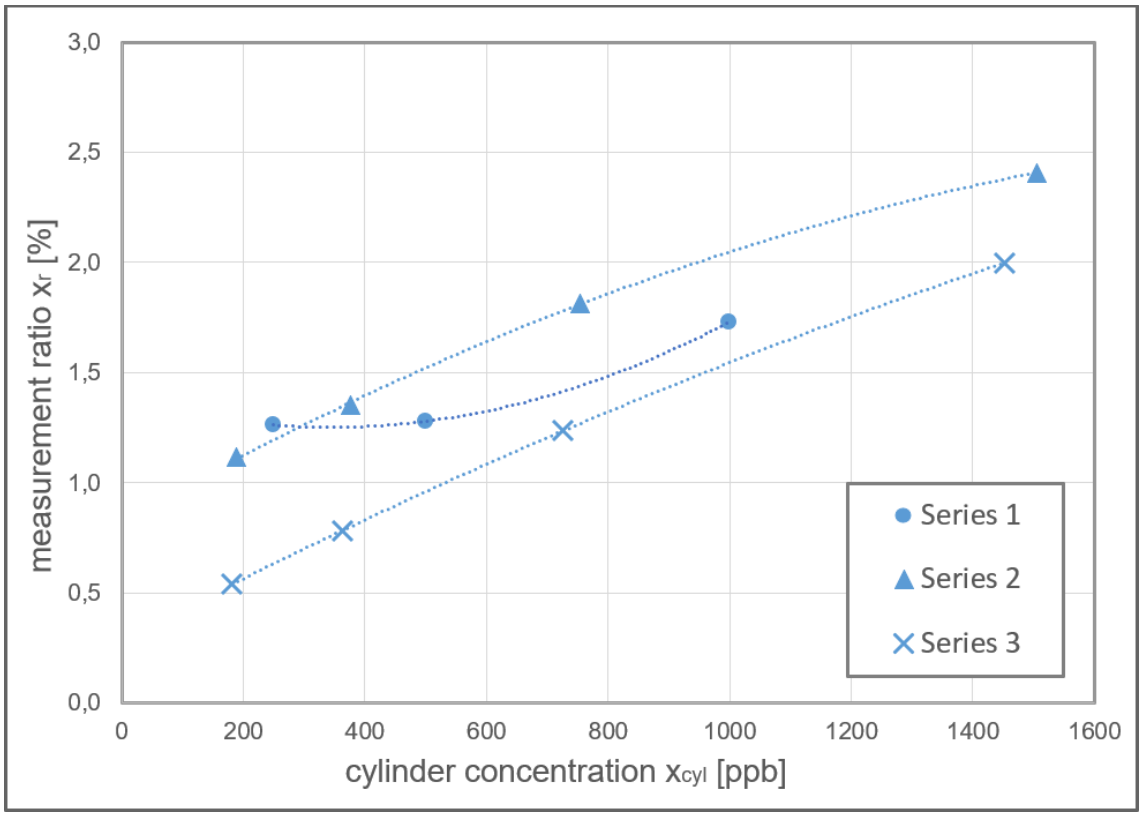

Figure 6.11, sensor qualification tests – UniTec SENS-IT Benzene

The graph shows large variations between the measurement ratios, with a reduction in response at low concentrations. Additionally, all tests showed a similar response curve as shown in Fig. 6.10. Thus, the response characteristics of the SENS-IT are similar to those of the Dräger sensor, indicating sorption processes. At the same time, contamination of the cell should not be possible due to the heated measuring cell. The rapid decay behavior with decay times between 40 s and 80 s of the sensor is also an indication that the inertia in the response behavior does not come from the sensor. Therefore, it is assumed that sorption processes in the unheated tube between the cuvette and the SENS-IT are responsible for the observed deviations.

6.5 Summary

The data evaluation of the qualification tests of the test stand regarding the provision of the calibration gas have shown that the selection of a suitable temperature and material is decisive for the quality of the measurement. The investigation of the temperature influence when using the Teflon cylinder showed a reduction of the uncertainty by increasing the temperature. By replacing the Teflon cylinder with the stainless-steel cylinder, the uncertainties were further reduced. Thus, the best results were obtained with the stainless-steel cylinder at 165 °C.

An analysis of the uncertainties of the calibration gas production showed uncertainties of less than ±1.5 % for molar fractions between 7.5 and 30 ppm. The weighing process had the greatest influence on the overall uncertainty. Based on these findings, sensor qualification tests were carried out. However, no satisfactory results could be achieved in these tests. While the deviations in the Dräger sensor are due to sorption processes in the sensor, the problems in the calibration of the SENS-IT are due to sorption processes in the test setup, which have a greater influence due to the lower gas concentrations. However, other properties such as the decay behavior and the high sensitivity demonstrate the sensor's suitability for the measurement task.

In order to achieve accurate calibration of the SENS-IT, three approaches were devised to reduce the uncertainties caused by sorption. The first approach involves the removal of the UV spectrophotometer from the test rig, as this is not suitable for measuring concentrations in the ppb range anyway due to the background noise of the measured value. On the one hand, this makes it possible to significantly shorten the tubes and thus reduce the surface area for the sorption processes, and on the other hand, the temperature can be increased to up to 200 °C, which may lead to a further reduction in adsorption.

The second approach is based on using a larger sample container with smaller wall-to-volume ratio, as this significantly influences the effect of sorption on the gas mixture. In addition, filling it with the same amount of HTF would directly lead to lower concentrations, saving dilution steps. The slower pressure drop at the same volume flow also improves the controllability of the volume flow and reduces the wall concentration at the end of an experiment, since the adsorbate has more time to desorb.

For the third approach, a whole new experimental setup must be created allowing continuous production of the calibration gas. For this purpose, a pump delivers small quantities of HTF into a heated nozzle in which the HTF is vaporized. The HTF is then mixed with a stream of air flowing around the nozzle before passing the sensor. The advantage of a continuous calibration gas supply is the adsorption-desorption equilibrium, reached after a certain time whereupon the gas concentration is no longer influenced by the surface. At the same time, pumping and measuring these small volume flows with acceptable uncertainties is a major challenge.

7 Prototype

In order to investigate the suitability of the SENS-IT sensor for the leakage measurement system presented in chapter 2.4 and to avoid possible errors in the design of the measurement system, a prototype was developed and built concluding this thesis. It is intended to be an image of the system's measurement section and to contain the main components of it. By injecting an HTF air mixture into the air flow of the prototype, a realistic measurement should be feasible. However, the focus is not on the collection of measured values with small deviations, but on the investigation of the interaction of the components. The schematic structure of the prototype can be seen in Figure 7.1.

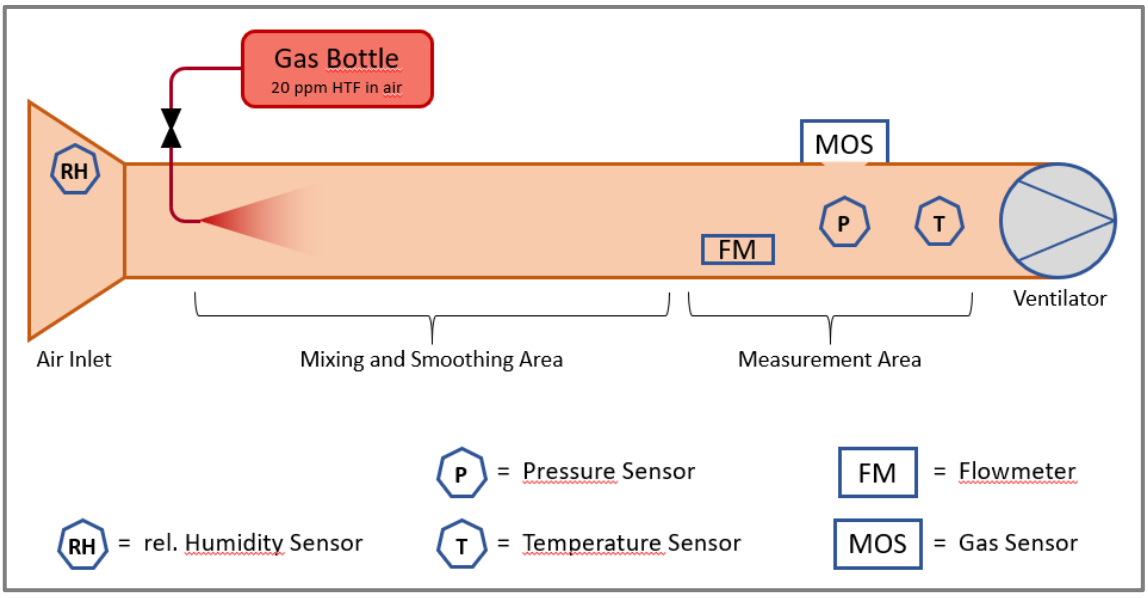

Figure 7.1, prototype - schematic setup

The prototype consists mainly of a long pipe divided into the mixing section, in which the gas is introduced and distributed homogeneously in the air, and the measuring section, where various sensors for monitoring the gas flow and a fan for generating the air flow are installed. A Raspberry Pi acquires the sensor readings and controls the fan as needed. During an experiment, the SENS-IT sensor determines the concentration of HTF in the air flow. The volume flow in the pipe is then adjusted based on the concentration values so that the concentration is within the measuring range of the SENS-IT. Using the volume flow, the pressure and the temperature, the mass flow can then be calculated. Based on the total mass flow and the HTF concentration, the mass flow of the HTF can then be calculated, which represents the leakage flow.

When selecting the components, special care was taken to ensure that they run on a minimum of 12 VDC, so that operation with a battery is possible. The electrical wiring of the components to the Raspberry Pi can be seen in Figure 7.2.

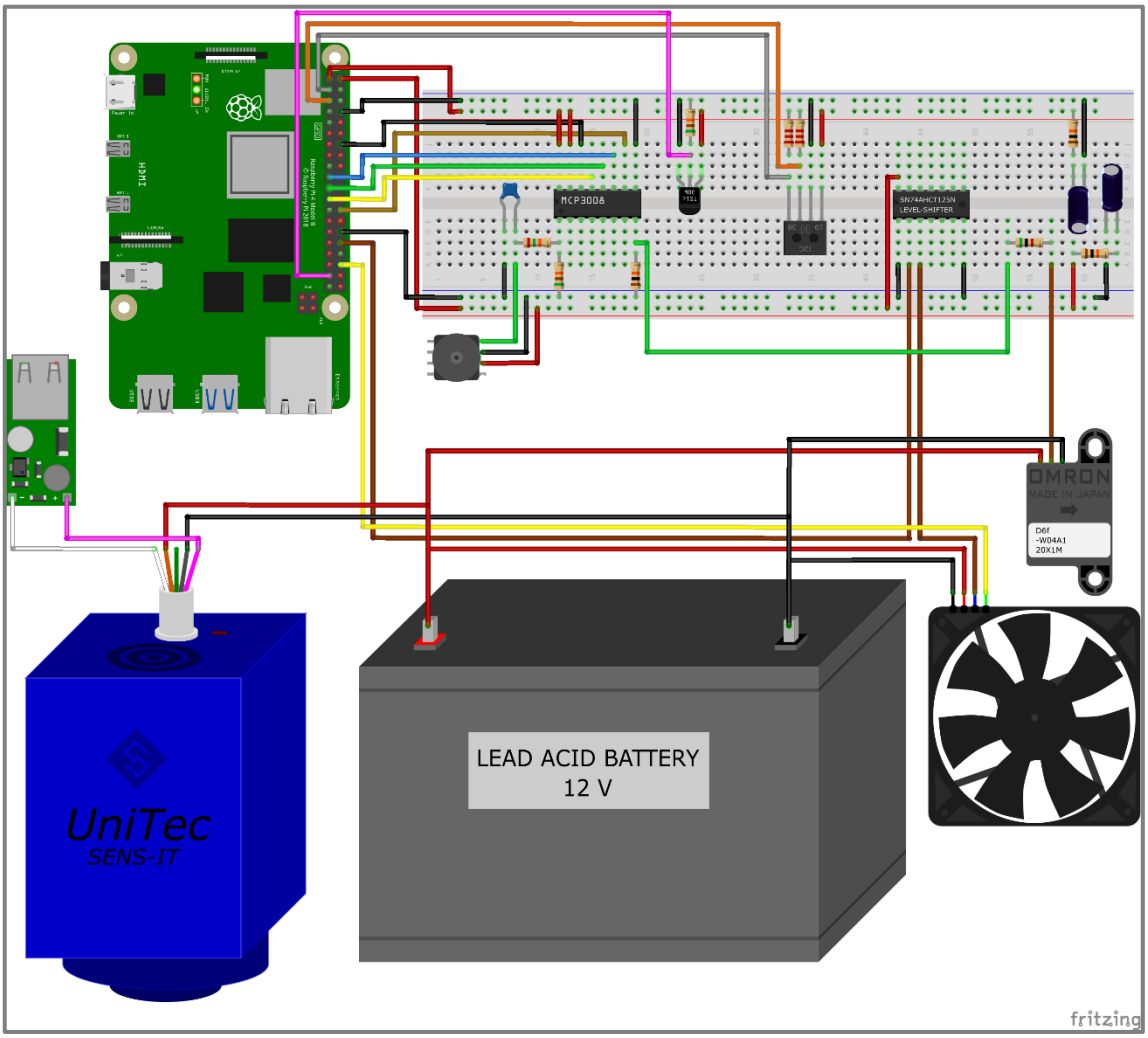

Figure 7.2, prototype - cabling of components

7.1 Data processing and software

The calculations are performed by the Raspberry Pi in real time. For this purpose, a program was written in Python that reads out and evaluates the measured values of all sensors. The data is then summarized in a .csv file to enable subsequent analysis. To facilitate possible changes to the prototype, such as replacing a sensor, the program was built in an object-oriented manner. This means that each sensor and actuator has its own subprogram in which its functions are stored. If, for example, another temperature sensor of the same type is to be installed, a second instance of this sensor can simply be created and integrated into the main program.

7.2 Usage

To operate the Raspberry Pi, for example for initiating a measurement, either a screen and a mouse must be connected, or a connection from a laptop with the VNC Viewer must be established. This has the advantage that no external power supply is required. In the future, installing a touchscreen would be useful so that the prototype does not need any other devices. Regarding the test conditions it is important that tests with the prototype should always be carried out outdoors, as the SENS-IT sensor is very sensitive to indoor air. However, due to the open wiring, it must always be protected from rain.

The HTF can be introduced into the mixing section using the cylinder already used in the previous experiments. For this purpose, a gas mixture with a comparatively high HTF concentration must be set in the cylinder, which is then injected into the air stream at the inlet of the measuring channel at a constant flow rate.

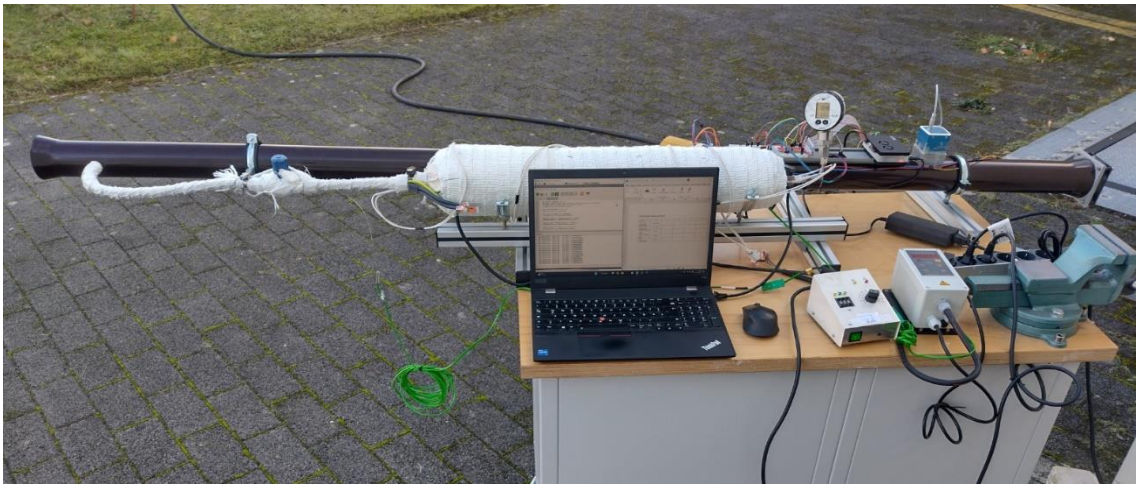

Figure 7.3, prototype test setup

Initial tests with the prototype confirmed the function of all sensors and the plausibility of the measured values. The control of the fan based on artificially generated sensor signals has also already been tested. In another test, its setup depicted in Figure 7.3, a gas mixture of HTF and synthetic air has already been introduced into the system. However, there were problems with the metering valve, whereupon the tests had to be aborted.

8 Conclusion and outlook

A test stand was developed to investigate the suitability of gas sensors for quantifying BP/DPO vapors in air. For this purpose, the calibration gas mixture is produced by weighing a 2 mg HTF droplet into a sample cylinder of 3.8 liters, then pressurized with air. This gas mixture is fed with a constant volume flow to the measuring cell of the sensor. The volume flow is adjusted and monitored using a metering valve between the cylinder and the measuring point and a flow meter downstream of the measuring cell. The setup is trace-heated to a constant temperature up to 165°C to avoid undesired condensation. To analyze the sensor behavior in the event of concentration changes, it is possible to switch between the calibration gas and the reference gas via a three-way valve. The influence of gas wall partitioning is minimized by selecting a Teflon-coated sample cylinder, lines and fittings made of Teflon, as well as by locating the measuring point as close to the cylinder as possible. In addition, to remove residues from previous tests and to clean the system, the system can be purged with reference gas, evacuated and heated.

Synthetic air is used as the reference gas in order to obtain conditions as close as possible to those in use, while excluding uncertainties due to fluctuating compositions or humidity. The required concentrations are generated by evaporating 2 mg HTF followed by a multi-stage dilution with synthetic air. By optimizing the manufacturing process in the lab, the calibration gases with BP/DPO kept between 7.5 ppm and 30 ppm have uncertainties of $u_{x,cyl} < 1.5\ \%$.

Prior to the tests to qualify the sensors, the system behavior of the test stand was investigated with regard to the concentration ratio between the measuring point and the cylinder as well as the temporal course. By heating the entire test stand and using a second uncoated stainless-steel cylinder, the influences of temperatures up to 165 °C and different materials on the system behavior of the test stand were investigated. A UV spectrophotometer with a heated flow-through cuvette with 100 mm path length was used to measure the HTF concentration at the measuring point. When considering the uncertainty of the concentration determination, an uncertainty of the absolute concentration value of 6.06 % was found, mainly caused by the uncertainty of the absorptivity coefficient for HTF of 6 %. However, since the uncertainty of the parameter leads to a constant relative deviation independent of the experimental conditions and the random deviation of the measured value is <1 %, the UV spectrophotometer is well suited for the evaluation of the influences. The test stand showed the least deviations when using the uncoated stainless-steel cylinder at a temperature of 165 °C, so these parameters were also used for the qualification of the sensors.

The objective of this thesis includes the qualification of sensors for the measurement of BP/DPO vapor in air as well as the analysis of suitable operating conditions to achieve good measurement accuracy in a leakage measurement system. The findings for good operating conditions from the qualification of the test stand can also be applied to the operating conditions of a leakage measurement system.

When examining two sensors for measuring BP/DPO vapors, both sensors were able to detect the vapors and also quantify them. However, the problem with the Dräger X-am 8000 is that the sensor reacts very slowly to changes in concentration, possibly due to sorption processes inside the sensor, and does not return to zero value after measuring BP/DPO. The UniTec SENS-IT Benzene sensor does not have this problem, as it has a heated measuring cell and a well-designed intake area for the HTF. Nevertheless, an accurate calibration of the sensor was not possible, since the test stand does not show sufficient accuracy at concentrations in the lower ppb range, in which the sensor operates.

These uncertainties are caused by the multi-stage dilution process that is carried out to achieve the low concentrations, as well as by the fact that the sorption processes with the cylinder and pipe walls have a greater influence on the gas mixtures with low concentrations. To reduce the uncertainties in the production of low concentrations, three optimization approaches were elaborated. Approach one follows the idea of reducing the amount of sorption by further increasing the temperatures and reducing the surface area of the lines. The plan of approach two is to use a larger sample cylinder to increase the ratio of adsorbent to surface area on the one hand, and to extend the duration of the experiment on the other hand. The advantage of the longer experiment duration is that after a certain time saturation occurs on the walls, which means that the gas flowing past is not affected any further. This is also the background of approach three, which involves the development of a new test rig for continuous calibration gas generation.

After the general qualification of the SENS-IT sensor, a prototype of the measuring section of the leakage measuring system was developed. It has all the components of the measuring section and is therefore not only able to test the sensor under realistic conditions, but also to validate the measuring concept of the leakage measuring system. Initial tests with the prototype have shown ...

In the further course of the project, the test stand should first be optimized on the basis of the knowledge gained so that a calibration of the SENS-IT is possible with low uncertainties. Subsequently, testing and optimization of the prototype is recommended in order to generate further findings for the development of the leakage measurement system.

References

Almasy, F. & Laemmel, H. (1950): Der Einfluss der Temperatur auf ds Absorptionsspektrum des Diphenyldampfes im nahen Ultraviolett. Extinktionsmessung zwischen 170 und 520 °C. *Fasciculis VII* 33, 2092–2100.

Arinaldo, Deon & Pujantoro, Mentari (2019): Levelized Cost of Electricity. 8.

ATS (2021): Thermal Pak Flexible Ball Joints. https://www.advancedthermal.net/wp-content/uploads/2021/05/ATSBallJointCatalog.pdf [Status 2022-05-27].

Bathen, D. et al. (2000): Emission of High-quality Pipework Flange Gaskets. *Chemical Engineering & Technology* 23, 11, 997–999.

Benoit, H. et al. (2016): Review of heat transfer fluids in tube-receivers used in concentrating solar thermal systems: Properties and heat transfer coefficients. *Renewable and Sustainable Energy Reviews* 55, 298–315.

Chan, Hui Ling et al. (2022): Understanding the Adsorption and Desorption of Sitagliptin Phosphate Monohydrate on SS2343, Glass, and PTFE Using QCM-D and Raman Spectroscopy. *Langmuir* 38, 34, 10575–10584.

Cozzi, Laura, Gould, Tim & Birol, Fatih (2020): World Energy Outlook 2020. 464.

Deming, Benjamin L. et al. (2019): Measurements of delays of gas-phase compounds in a wide variety of tubing materials due to gas–wall interactions. *Atmospheric Measurement Techniques* 12, 6, 3453–3461.

DLR (2021): Solar thermal power plants - Heat, electricity and fuels from concentrated solar power, Cologne: German Aerospace Center (DLR) Institute of Solar Research. https://www.dlr.de/sf/en/PortalData/73/Resources/dokumente/publikationen_medien/dlr_und_sf/Study_Solar_thermal_power_plants_DLR_2021-05.pdf.

Dow Chemical Company (2022): Technical Data Sheet - Dowtherm A Heat Transfer Fluid. https://www.dow.com/en-us/document-viewer.html?docPath=/content/dam/dcc/documents/en-us/productdatasheet/176/176-01463-01-dowtherm-a-tds.pdf [Status 2022-11-3].

Dräger (2020): Dräger X-am 8000. https://www.draeger.com/Products/Content/x-am-8000-pi-9103261-de-master.pdf [Status 2022-11-13].

Eastman (2020): Safety Data Sheet - Therminol® VP1 Heat Transfer Fluid. https://ws.eastman.com/ProductCatalogApps/PageControllers/MSDSAll_PC.aspx?product=71093459 [Status 2022-05-23].

Eastman (2019): Technical Data Sheet - Therminol® VP1 Heat Transfer Fluid. https://productcatalog.eastman.com/tds/ProdDatasheet.aspx?product=71093459 [Status 2021-10-18].

Fatih, Birol (2020): World Energy Outlook 2020 - press release, Internationlal Energy Agency. https://www.iea.org/news/world-energy-outlook-2020-shows-how-the-response-to-the-covid-crisis-can-reshape-the-future-of-energy [Status 2022-05-17].

FITOK (2022): Sampling Assemblies, Sample Cylinders and Accessories. 290, 6, 9–23.

Grirate, H. et al. (2016): Life time analysis of thermal oil used as heat transfer fluid in CSP power plant. In SOLARPACES 2015: International Conference on Concentrating Solar Power and Chemical Energy Systems. Cape Town, South Africa, 040005. http://aip.scitation.org/doi/abs/10.1063/1.4949096 [Status 2022-05-26].

Hardelt, Marcel (2022): Design of a leak measurement system for flexible pipe connectors in solar power plants.

Harris, Phil, Pelligrini, Mike & Corp, OBrien (2004): MASS TRANSPORT IN SAMPLE TRANSPORT LINES ADSORPTION DESORPTION EFFECTS AND THEIR INFLUENCE ON PROCESS ANALYTICAL MEASUREMENTS. 12.

Heller, Peter W. (Ed.) (2017): The performance of concentrated solar power (CSP) systems - analysis, measurement and assessment, Cambridge, MA: Woodhead Publishing, an imprint of Elsevier.

Hilgert, C. et al. (2015): REPA Teststand. 2.

Hilgert, Christoph et al. (2019): Qualification of silicone based HTF for parabolic trough collector applications. *AIP Conference Proceedings* 2126, 1, 080003.

IRENA (2021): Renewable Power Generation Costs in 2020, Abu Dhabi: International Renewable Energy Agency. https://www.irena.org/publications/2021/Jun/Renewable-Power-Costs-in-2020 [Status 2022-05-18].

JCGM (2008): Evaluation of measurement data - Guide to the expression of uncertainty in measurement. 120.

Jousten, Karl (Ed.) (2018): Handbuch Vakuumtechnik, Wiesbaden: Springer Fachmedien Wiesbaden. http://link.springer.com/10.1007/978-3-658-13386-3 [Status 2022-11-7].

Jung, C. et al. (2015): Technological Perspectives of Silicone Heat Transfer Fluids for Concentrated Solar Power. *Energy Procedia* 69, 663–671.

Krishna, Yathin et al. (2020): State-of-the-art heat transfer fluids for parabolic trough collector. *International Journal of Heat and Mass Transfer* 152, 119541.

Lang, C. & Lee, B. (2015): Heat Transfer Fluid Life Time Analysis of Diphenyl Oxide/Biphenyl Grades for Concentrated Solar Power Plants. *Energy Procedia* 69, 672–680.

Leidinger, M. et al. (2014): Selective detection of hazardous VOCs for indoor air quality applications using a virtual gas sensor array. *Journal of Sensors and Sensor Systems* 3, 2, 253–263.

León, Javier et al. (2018): Test loop for inter-connections of parabolic trough collectors. In SolarPACES 2017: International Conference on Concentrating Solar Power and Chemical Energy Systems. Santiago, Chile, 030008. http://aip.scitation.org/doi/abs/10.1063/1.5067024 [Status 2022-05-22].

Li, D., Xie, M. & Neumann, A. W. (1993): Vapour adsorption and contact angles on hydrophobic solid surfaces. *Colloid and Polymer Science* 271, 6, 573–580.

Lovegrove, Keith & Stein, Wes (2021): Concentrating solar power technology - principles, developments, and applications, Elsevier. https://linkinghub.elsevier.com/retrieve/pii/B9780128199701099916 [Status 2022-05-16].

Matsunaga, Aiko & Ziemann, Paul J. (2010): Gas-Wall Partitioning of Organic Compounds in a Teflon Film Chamber and Potential Effects on Reaction Product and Aerosol Yield Measurements. *Aerosol Science and Technology* 44, 10, 881–892.

Mehos, Mark et al. (2020): Concentrating Solar Power Best Practices Study, https://www.nrel.gov/docs/fy20osti/75763.pdf [Status 2022-05-27].

Mir-Artigues, Pere, del Río, Pablo & Caldés, Natàlia (2019): The Economics and Policy of Concentrating Solar Power Generation, Cham: Springer International Publishing. http://link.springer.com/10.1007/978-3-030-11938-6 [Status 2022-05-16].

Montes, M. J., Abánades, A. & Martínez-Val, J. M. (2010): Thermofluidynamic Model and Comparative Analysis of Parabolic Trough Collectors Using Oil, Water/Steam, or Molten Salt as Heat Transfer Fluids. *Journal of Solar Energy Engineering* 132, 2, . https://doi.org/10.1115/1.4001399 [Status 2022-11-3].

NIST (2019): The NIST reference on Constants, Units, and Uncertainty - molar gas constant,. https://physics.nist.gov/cgi-bin/cuu/Value?r [Status 2022-11-27].

NIST, National Institute of Standards and Technologie (2022): Diphenyl ether - UV/Visible spectrum, NIST Chemistry WebBook. https://webbook.nist.gov/cgi/inchi?ID=C101848&Mask=400#UV-Vis-Spec [Status 2022-11-17].

NPI (2009): NPI Volotile Organic Compound Definition and Information. 5.

Omiya, Yuya & Sawa, Toshiyuki (2014): Stress Analysis and Sealing Performance Evaluation of Bolted Pipe Flange Connections With Smaller and Larger Nominal Diameter Under Repeated Temperature Changes. In ASME 2014 Pressure Vessels and Piping Conference. American Society of Mechanical Engineers Digital Collection. https://risk.asmedigitalcollection.asme.org/PVP/proceedings/PVP2014/45998/V002T02A003/279284 [Status 2021-10-29].

Pagonis, Demetrios et al. (2017): Effects of gas-wall partitioning in Teflon tubing and instrumentation on time-resolved measurements of gas-phase organic compounds. *Atmospheric Measurement Techniques* 10, 4687–4696.

Persson, B N J & Yang, C (2008): Theory of the leak-rate of seals. *Journal of Physics: Condensed Matter* 20, 31, 315011.

Pfeiffer Vakuum (2014): Lecksucher Kompendium. 84.

Pitz-Paal, Robert (2020): Concentrating Solar Power. In *Future energy: improved, sustainable and clean options for our planet*. 413–430.

Plass-Duelmer, Christian, Sassi, Guido & Sauerwald, Tilman (2017): Metrology for VOC indicators in air pollution and climate change. *EURAMET* 39.

Plumpe, Andreas (2016): Design of a Test Rig and its Testing Methods for Rotation and Expansion Performing Assemblies in Parabolic Trough Collector Power Plants.

Pörtner, H.-O. et al. (2022): Climate Change 2022 - Impacts, Adaptation and Vulnerability: Summary for Policymakers, IPCC. https://www.ipcc.ch/report/ar6/wg2/resources/spm-headline-statements/ [Status 2022-05-16].

Schiffer, H.-W. et al. (2021): Energie in der Welt - Zahlen und Fakten. https://www.weltenergierat.de/publikationen/energie-fuer-deutschland/energie-fuer-deutschland-2021/energie-in-der-welt-zahlen-fakten/ [Status 2022-05-17].

Skoog, Douglas A., Holler, F. James & Crouch, Stanley R. (2017): Principles of Instrumental Analysis, Cengage Learning.

Sniderman, Debbie (2011): Moving Hot Fluids Through Solar Troughs,. https://www.asme.org/topics-resources/content/Moving-Hot-Fluids-Through-Solar-Troughs [Status 2022-05-22].

Solartechadvisor (2022): Heat Transfer Fluids Used For CSP (Concentrated Solar Power Systems),. https://solartechadvisor.com/csp-heat-transfer-fluids/ [Status 2022-11-3].

Solutia (1999): Technical Data Sheet - Therminol® VP1 Heat Transfer Fluid. https://productcatalog.eastman.com/tds/ProdDatasheet.aspx?product=71093459 [Status 2021-10-18].

Spinelle, Laurent et al. (2017): Review of Portable and Low-Cost Sensors for the Ambient Air Monitoring of Benzene and Other Volatile Organic Compounds. *Sensors* 17, 7, 1520.

Sun, Jie et al. (2020): Comprehensive Review of Line-Focus Concentrating Solar Thermal Technologies: Parabolic Trough Collector (PTC) vs Linear Fresnel Reflector (LFR). *Journal of Thermal Science* 29, 5, 28.

Szulczyński, Bartosz & Gębicki, Jacek (2017): Currently Commercially Available Chemical Sensors Employed for Detection of Volatile Organic Compounds in Outdoor and Indoor Air. *Environments* 4, 1, 21.

The World Bank (2019): Solar Resource Map - Direct Normal Iradiation. https://solargis.com/maps-and-gis-data/download/world [Status 2022-05-17].

UniTec (2022): SENS-IT-Datasheet. http://www.unitec-srl.com/site/wp-content/uploads/2014/11/SENS-IT-Datasheet_06_18.pdf [Status 2022-10-21].

UniTec (2020): SENS-IT-Operating_manual. http://www.unitec-srl.com/site/wp-content/uploads/2015/04/SENS-IT-Datasheet.pdf [Status 2020-05-13].

US EPA, OAR (2014): Technical Overview of Volatile Organic Compounds,. https://www.epa.gov/indoor-air-quality-iaq/technical-overview-volatile-organic-compounds [Status 2022-05-30].

Vaittinen, O. et al. (2014): Adsorption of ammonia on treated stainless steel and polymer surfaces. *Applied Physics B* 115, 2, 185–196.

WACKER HELISOL® – A New Silicone Based Heat Transfer Fluid.

Wiegleb, Gerhard (2016): Gasmesstechnik in Theorie und Praxis: Messgeräte, Sensoren, Anwendungen, Wiesbaden: Springer Fachmedien Wiesbaden. http://link.springer.com/10.1007/978-3-658-10687-4 [Status 2022-11-18].

Zarza Moya, E. (2017): Innovative working fluids for parabolic trough collectors. In *Advances in Concentrating Solar Thermal Research and Technology*. Elsevier, 75–106. https://linkinghub.elsevier.com/retrieve/pii/B9780081005163000058 [Status 2022-11-3].

Zhang, X. et al. (2015): Vapor wall deposition in Teflon chambers. *Atmospheric Chemistry & Physics* 15, 4197–4214.

Terminology and abbreviations

BP/DPO	Biphenyl / Diphenyl Oxide
CIEMAT	Centro de Investigaciones Energéticas, Medioambientales y Tecnológicas (Center for Energy, Environment and Technology Research)
CSP	Concentrated Solar Power
DLR	Deutsches Zentrum für Luft- und Raumfahrt e.V. (German Aerospace Center)
DSG	Direct Steam Generation
HTF	Heat Transfer Fluid
IEA	International Energy Agency
LCOE	Levelized Cost of Electricity
MOS	Metal Oxide Semiconductor (sensor technology)
PID	Photo Ionizations Detector (sensor technology)
PSA	Plataforma Solar de Almería
PTC	Parabolic Trough Collector
PV	Photovoltaic
REPA	Rotation and Expansion Performing Assembly
VOC	Volatile Organic Compound

Symbols and variables

Symbol	Unit	Description
A	-	absorbance
b	cm	path length (cuvette)
c	mol/l	concentration (molar)
I	W/m²	intensity of emitted light
I_0	W/m²	intensity of incident light
m	kg	mass
M_i	kg/mol	individual molar mass
n_i	mol	individual mount of substance
p	Pa	pressure
R	J/(mol·K)	molar gas constant
T	-	transmittance
T	K	Temperature
t_{dec}	s	Decay time
t_{pur}	s	Purification time
t_{res}	s	Response time
t_{ret}	s	Retention time
V	m³	volume
x_i	mol/mol	individual mole fraction
x_{UV}	mol/mol	mole fraction of HTF in air measured by the UV-spectrophotometer
x_{cyl}	mol/mol	mole fraction of HTF in air in the cylinder
ε	cm²/mol	absorptivity

List of figures

Appendencies

Appendix A, Laboratory test stand

Declaration of originality

I hereby affirm that I have independently written this work and have not used any publications, templates or aids other than those I have indicated. All parts of my work which have been taken literally or correspondingly from other publications have been duly acknowledged. This also applies to Internet sources. I affirm that I have not previously submitted this work or any unquoted parts thereof in any other examination procedure. I am aware that my work can be checked by means of plagiarism recognition software in order to verify the integrity of its written content. I also affirm you that the electronic form is identical to the printed version.

Köln, 01 December 2022